11. Nanoparticles and Their Applications

Seyedsina Moeinzadeh, Esmaiel Jabbari

Nanoparticles (NPs) are synthesized from several classes of materials including inorganic, organic, hybrid and biological materials. Inorganic NPs are synthesized by ball milling, vapor deposition, electrospraying, reduction of metal salts, sol–gel, coprecipitation and thermal decomposition. Organic NPs are synthesized by microemulsion, nanoprecipitation, dialysis and rapid expansion of supercritical solutions. Hybrid NPs are synthesized from both organic and inorganic materials. There are a number of naturally occurring biological NPs including lipoproteins, exosomes, ferritin, and viruses. Further, NPs can be synthesized from biomolecules including proteins, peptides and polysaccharides. The surface to volume ratio, superparamagnetism, hardness, Coulomb energy and catalytic activity of NPs are generally higher than those of bulk materials. Due to their unique structural, magnetic, mechanical and electrical properties, NPs are used in a wide range of applications including biosensing, drug delivery, bioimaging, catalysis, nanomanufacturing, lubrication, electronics, textile manufacturing, and water treatment systems. This chapter covers the classification, synthesis, properties and applications of NPs.

11.1 Overview

Nanoparticles (NPs) are solid colloidal particles with dimensions in the range of a few nanometers to a few hundred nanometers [11.1]. Due to their small size, NPs have significantly higher surface to volume ratios, hence different physicochemical properties compared with bulk materials. NPs have applications in a wide range of areas including [11.2]:

- Biosensing
- Drug delivery
- Bioimaging
- Catalysis
- Nanomanufacturing
- Lubrication
- Electronics
- Textile industry
- Water treatment.

In the first part of this chapter, various methods for the synthesis of inorganic, organic, hybrid, and biological NPs are described. The properties of NPs including size and morphology as well as their unique magnetic, mechanical and electrical properties are discussed next. The major applications of NPs are discussed in the last part of this chapter.

B. Bhushan (Ed.), *Springer Handbook of Nanotechnology*, DOI 10.1007/978-3-319-49347-3_11

11.2 NPs Classification and Synthesis

11.2.1 NPs Classification

Multiple approaches are used to classify nanoparticles into the following: two-dimensional (e.g., nanotubes) and three-dimensional (e.g., spherical NPs, dendrimers). NPs can be synthesized from several classes of materials including inorganic (e.g., metal oxide NPs), organic (e.g., polymeric NPs), hybrid and biological materials [11.3]. Hybrid NPs are comprised of an inorganic core with organic shell or an organic core with inorganic shell. NP synthesis falls into two major categories namely top-down and bottom-up synthetic approaches. In the top-down approach, NPs are synthesized from bulk materials using traditional solid-state techniques (e.g., milling, machining) or lithographic techniques. In the bottom-up approach, NPs are synthesized from single molecules via chemical reactions, self-assembly, aggregation or chemical vapor deposition [11.1].

11.2.2 NPs Synthesis

Inorganic NPs

Depending on the type of material and the desired NP size, different physical or chemical strategies can be used to synthesize inorganic NPs [11.1]. Here, a number of physical techniques (ball milling, vapor deposition and electrospraying) and chemical methods (reduction of metal salts, sol-gel, coprecipitation and thermal decomposition) are described for the synthesis of inorganic NPs. The microemulsion technique that is extensively used for the synthesis of both organic and inorganic NPs is described in the section on organic NPs.

The ball milling method is a physical top-down synthesis approach based on breaking of solid particulate materials into smaller particles using high-energy balls rotating within a closed chamber [11.1]. Metal and metal oxide NPs have been synthesized using the ball milling method [11.4, 5]. The size and physicochemical characteristics of NPs synthesized via ball milling depend on milling time, rotation speed, ball to powder weight ratio as well as temperature and pressure [11.1]. For example, magnetite (Fe_3O_4) NPs with sizes ranging from 12 to 20 nm were synthesized via ball milling of iron powder in the presence of distilled water [11.5]. The size of Fe_3O_4 NPs decreased and the purity of NPs increased with increasing milling time from 10 to 96 h [11.5].

Vapor deposition is a physical approach for the synthesis of NPs based on vaporization of the material from a solid source using an ion (sputtering), electron (electron beam evaporation) or laser (laser ablation) beam followed by nucleation and growth of the vaporized material on a substrate (Fig. 11.1) [11.1]. Metal and metal oxide NPs have been synthesized via the vapor deposition method. For example, pure metallic (Fe, Ag, Au, Y, Co), nonmetallic (C) and metal oxide (TiO_2) NPs were synthesized via sputtering-based vapor deposition on a direct current (DC) magnetron cathode [11.6]. The size and physicochemical characteristics of NPs synthesized by vapor deposition are affected by [11.6]:

- Target to substrate distance
- Type of substrate
- Substrate temperature
- Deposition time
- Chamber pressure
- Electrical power.

In the laser-based vapor deposition method, the number of pulses, deposition time, gas pressure and substrate temperature significantly affects the size and morphology of NPs [11.7, 8]. For instance, the average size of FeCo NPs synthesized by pulsed laser vapor deposition increased from 4.8 to 8.6 nm as the argon

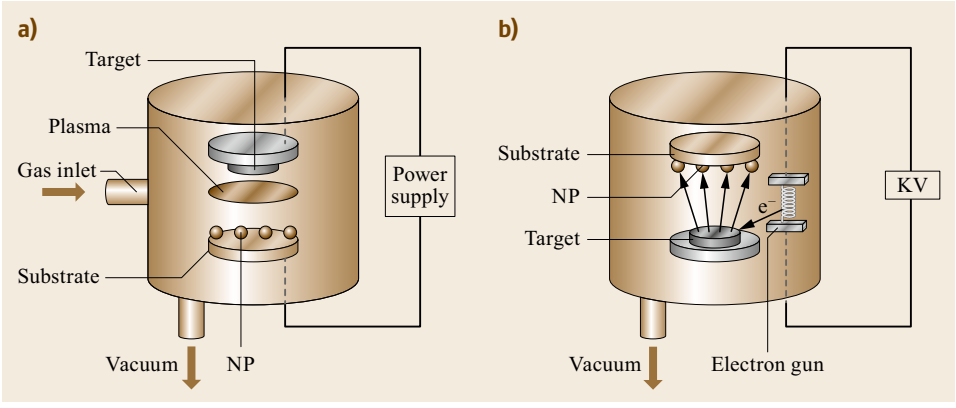

Fig. 11.1a,b Schematic representation of the physical vapor deposition method using **(a)** ion and **(b)** electron beams

gas pressure inside the chamber increased from 10 to 90 kPa [11.7]. Further, agglomeration of the FeCo NPs was reduced by increasing the temperature gradient [11.7].

In the electrospraying method, nanodroplets of a solution of the selected material are sprayed from a syringe to a collector within a high electric field (Fig. 11.2) [11.9]. Metal, metal oxide and polymer NPs have been synthesized via electrospraying [11.9–11]. A number of solvents including toluene, ethanol, methanol and isopropyl alcohol have been used for electrospraying of inorganic NPs [11.1]. For example, Sn NPs with an average size of 3 nm were synthesized by electrospraying a solution of $SnCl_2 \cdot 2H_2O$ in isopropyl alcohol into a reductive bath [11.10]. Monodisperse gold NPs with 5.7 nm diameter were synthesized by electrospraying $HAuCl_4 \cdot H_2O$ solution in isopropanol into a bath containing the reducing agent octadecylaminomethanol and the nonpolar solvent cyclohexane [11.11].

The most common chemical method for the synthesis of metallic NPs is reduction of metal ions in a metal salt solution using a reducing agent. Sodium borohydride ($NaBH_4$) and hydrazine (N_2H_4) are commonly used as reducing agents for the reduction of metal ions [11.12]. For example, the ferric ions in the solution of $FeCl_3 \cdot 6H_2O$ salt were reduced using sodium borohydride to synthesize iron NPs [11.13]. The size and morphology of NPs synthesized by the reduction method depends on temperature and pH of the reaction medium as well as the reactant concentration [11.14, 15].

The sol-gel technique has been used extensively for the synthesis of metal oxide NPs. The sol-gel method, can be divided into three major steps [11.12, 16]. In the first step (sol formation), the metal alkoxide or the metal salt is hydrolyzed in water/ethanol solution to form metal hydroxide (11.1). The metal hydroxide then undergoes condensation to create metal–O–metal bridges (11.2). For example, the hydrolysis and condensation reactions of tetraethylorthosilicate ($Si(OC_2H_5)_4$) in the synthesis of silica NPs are as follows

$$Si(OC_2H_5)_4 + 4(H_2O) \xrightarrow{\text{hydrolysis}} Si(OH)_4 + 4C_2H_5OH \quad (11.1)$$

$$Si(OH)_4 + Si(OH)_4 \xrightarrow{\text{condensation}} (OH)_3Si{-}O{-}Si(OH)_3 + H_2O \quad (11.2)$$

Colloidal particles or sol is formed when sufficient metal–O–metal bridges are created locally. Usually a mineral base (e.g., NH_3) or a mineral acid (e.g., HCl) is used as a catalyst. In the second step, colloidal particles link together with time to create a three-dimensional network at the nanoscale. In the third step, the nanoparticles are dried by heating, freeze drying or supercritical drying [11.16]. After drying and dehydration, NPs are densified by heat treatment at high temperatures [11.16].

Coprecipitation is another approach for the synthesis of inorganic and hybrid NPs [11.12, 17]. In the coprecipitation method, two or more water soluble salts react in aqueous solution to form a water insoluble salt that precipitates and forms NPs [11.12]. For example, hydrated ferrous chloride ($FeCl_2 \cdot 4H_2O$) and ferric chloride ($FeCl_3 \cdot 6H_2O$) undergo oxidative reaction following deprotonation in aqueous solution in the presence of $NH_3 \cdot H_2O$ as the precipitating agent [11.12]. The overall reaction can be written as

$$2Fe^{3+} + Fe^{2+} + 8OH^- \rightarrow Fe_3O_4 + 4H_2O\,. \quad (11.3)$$

When the concentration of Fe_3O_4 product in the solution increases above the solubility limit, the product precipitates by nucleation in the liquid phase. The growth of Fe_3O_4 crystals continues with precipitation reaction on the nucleating surfaces. Finally, the small particles undergo agglomeration via Ostwald ripening and form Fe_3O_4 NPs [11.12].

The thermal decomposition technique is used to synthesize metal oxide NPs from metal salts [11.12, 17]. In this method, a transition metal (e.g., Fe, Zn, Zr, and Co) salt is stabilized in an organic solvent/surfactant solution and mixed with an organic compound to form an organometallic complex. The organometallic complex is decomposed at high temperatures to create metal oxide NPs. A wide range of surfactants including oleylamine [11.18], oleic acid [11.19], benzylamine [11.20], and pentanedione [11.21] have been used to stabilize metal salts in the thermal decomposition process.

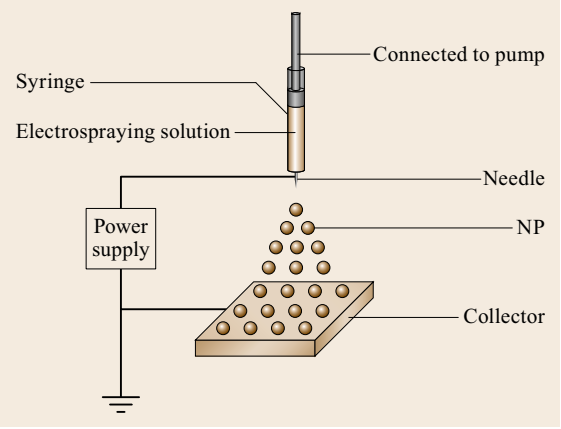

Fig. 11.2 Schematic representation of electrospraying method for the synthesis of NPs

Organic NPs

Several synthetic approaches for the synthesis of organic NPs are used. These include microemulsion, nanoprecipitation, dialysis and rapid expansion of a supercritical solution. The microemulsion method, used extensively for the synthesis of organic NPs, involves two major steps [11.22]. In the first step (emulsification), the organic compound (e.g., the polymer) is dissolved in a selective solvent and the polymer solution (dispersed phase) is emulsified in a second solvent (continuous phase) that is fully or partially immiscible in the dispersed phase solvent (Fig. 11.3). Nanodroplets of the disperse phase with diameters ranging from 10–500 nm are formed in the emulsification step [11.22]. There are two methods for the emulsification of the dispersed phase namely high-energy and low-energy methods. High-energy methods usually involve sonication or high-shear mixing [11.23]. The low-energy methods are divided into two groups: microemulsification based on spontaneous diffusion and microemulsification based on phase inversion stimulated by a change in temperature or composition [11.23, 24]. In the spontaneous emulsification of oil nanodroplets in water, the oily phase is composed of a partially immiscible solvent and a water soluble solvent, usually acetone or ethanol. When the oily and aqueous solutions are mixed, the water soluble solvent rapidly diffuses from the oily phase to the aqueous phase. This rapid diffusion between the two phases produces surface tension gradients that lead to the formation of a microemulsion [11.25].

The phase inversion techniques for microemulsification are classified into two groups: The so-called phase inversion temperature (PIT) method is centered on the hydrophilic-lipophilic transition of polyethylene glycol (PEG)-based surfactants at high temperatures as a result of disruption of the hydrogen bonding [11.24]. As shown in Fig. 11.4, an oil (dispersed phase)/water (continuous phase) emulsion at constant composition inverts to a water/oil emulsion when temperature rises above the inversion temperature [11.26]. The affinity of surfactants for oil and water phase is similar at the inversion temperature leading to a minimal interfacial tension and bicontinuous microemulsion in the transition region. Therefore, kinetically stable nanodroplets can be formed by rapid cooling or dilution of the aforementioned emulsion systems at invasion temperature [11.24] (Fig. 11.4). The second phase inversion technique for microemulsification, the so-called emulsion inversion point (EIP) method, employs emulsion composition change for phase transition. The water/oil emulsion is formed by successive addition of water to an oil solution. The emulsion undergoes phase transition from water/oil to oil/water with increasing volume fraction of water. A bicontinuous microemulsion with minimal interfacial tension and nanosized droplets is formed at the phase inversion point [11.26].

Following emulsification, the NPs are formed in the second step of the microemulsion technique from the emulsified nanodroplets via solvent removal, gelation, or emulsion polymerization (Fig. 11.3a). Different approaches including solvent evaporation and solvent displacement methods have been employed for solvent removal and precipitation of the NPs in

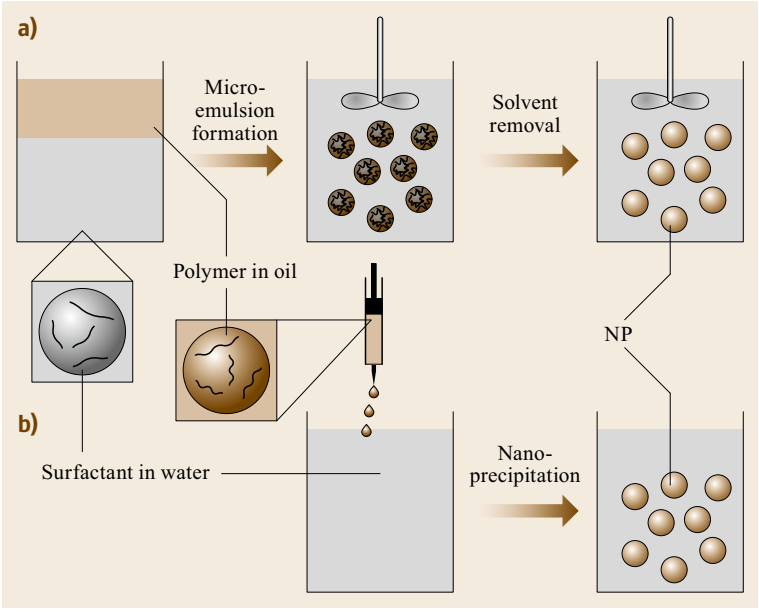

Fig. 11.3a,b Schematic representation of **(a)** microemulsion and **(b)** nanoprecipitation techniques for the synthesis of organic NPs

microemulsion systems [11.24]. In the solvent evaporation method, a volatile solvent (e.g., chloroform or dichloromethane) is used as the solvent in the disperse phase. The volatile solvent is evaporated under vacuum leaving the polymer in the nanodroplets. During solvent evaporation, the size of the nanodroplets initially decreases dramatically due to solvent loss and then increases significantly due to droplet coalescence [11.24]. Organic NPs from numerous polymers and copolymers including poly(lactide) (PLA), poly(lactide-co-glycolide) (PLGA), poly(ε-caprolactone) (PCL), and PEG-co-PLA were synthesized via the solvent evaporation method [11.27–29]. In the solvent displacement method, a solvent with partial miscibility in water is used in the disperse phase. NPs are formed by solvent displacement from the dispersed phase to the continuous aqueous phase upon successive addition of water or dialysis [11.24].

The gelation of macromolecules in the nanodroplets is another approach for the synthesis of NPs in microemulsion systems. Several gelation mechanisms depending on physicochemical properties of the macromolecules within the nanodroplets are employed for NP formation. These include temperature-sensitive physical gelation, pH-sensitive gelation and chemical crosslinking [11.30, 31]. For example, nanogels based on polyethylene glycol (PEG) macromers chain-extended with short lactide (L) and glycolide (G) segments were synthesized via dialysis method and they were used for grafting proteins (Fig. 11.5a) [11.32]. The size of synthesized nanogels ranged from 118 to 190 nm depending on the molecular weight of PEG and L/G molar ratio [11.32]. Further, the rate of BSA protein release from the nanogels was between 51% release after 24 days and complete release in 11 days depending on the molecular weight of PEG and L/G molar ratio (Fig. 11.5b) [11.32].

Polymerization of monomers in nanodroplets is used extensively for the synthesis of NPs from microemulsions. In the first step, nanodroplets of monomers with low water solubility are formed in the aqueous solution containing a surfactant and a water soluble initiator (Fig. 11.6). Free radical or ionic initiators are used depending on the type of polymerization reaction. The collision of initiator molecules and monomer molecules starts the polymerization reaction within the nanodroplets. Solid NPs are formed with the progress of polymerization reaction and increase in the molecular weight of the polymer molecules in the nanodroplets. NPs of different polymers including polystyrene (PS), poly(methyl methacrylate) (PMMA) and poly(vinylcarbazole) were synthesized using emulsion polymerization [11.2, 33, 34]. Further, surfactant-free emulsion polymerization has been employed for the synthesis of NPs based on acrylic or vinyl monomers [11.24]. For example, PMMA, PS and poly(vinyl acetate) (PVA)-based NPs with diameter ranging from 155 to 345 nm were synthesized using surfactant-free emulsion polymerization and sodium persulfate as the initiator [11.35]. The surfactant removal, an indisputable step in conventional emulsion polymerization, is absent in the surfactant-free emulsion polymerization technique, which is a significant advantage in large-scale manufacturing of organic NPs.

In addition to the conventional and surfactant-free emulsion polymerization, interfacial polymerization has been used for the synthesis of polymeric nanocap-

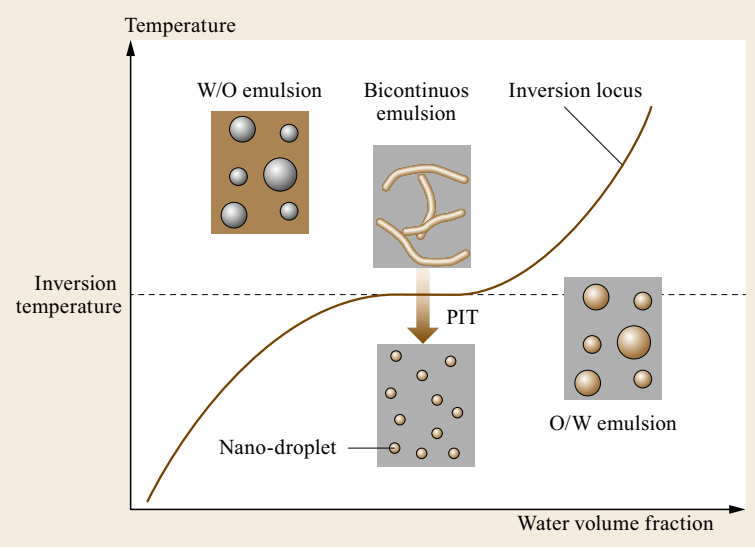

Fig. 11.4 Schematic representation of the phase inversion temperature (PIT) method for microemulsification. Nanodroplets are formed with rapid cooling of the bicontinuous emulsion. Reprinted with permission from [11.26]

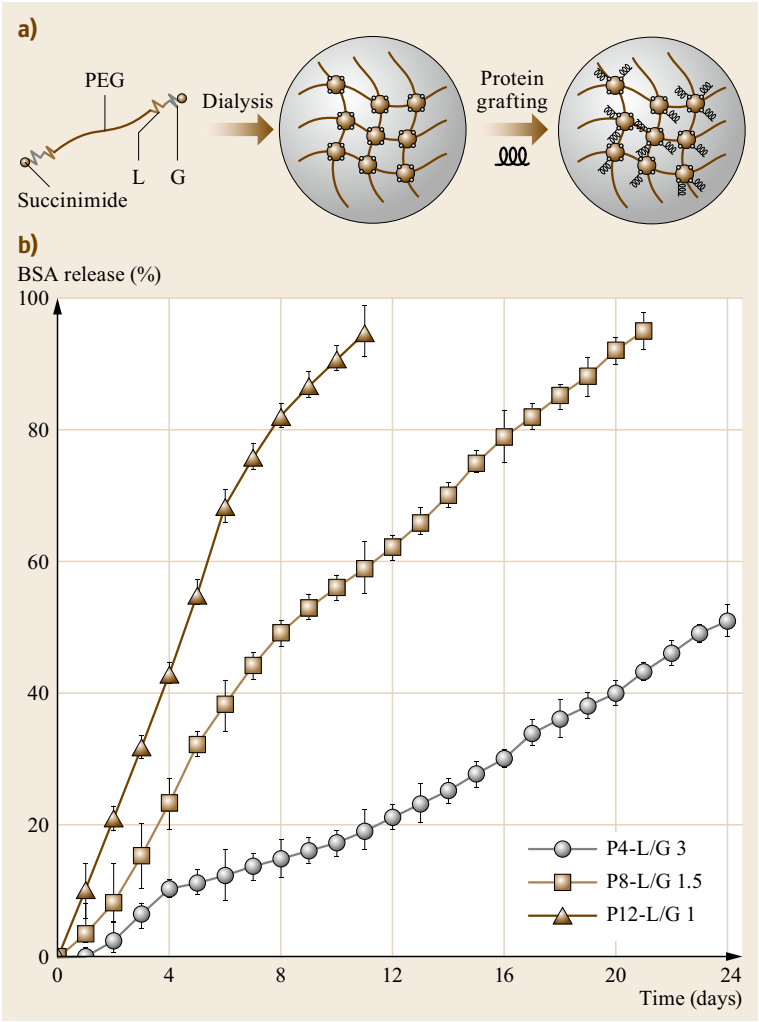

Fig. 11.5 **(a)** Schematic diagram for the assembly of nanogels from PEG macromers chain-extended with short lactide (L) and glycolide (G) segments and protein grafting to nanogels. **(b)** The cumulative BSA release from nanogels in PBS with incubation time. The abbreviations $P4$, $P8$, and $P12$ represent nanogels made from macromers with PEG $M_W = 4, 8$ and 12 kDa. The abbreviations $L/G\,3$, $L/G\,1.5$ and $L/G\,1$ represent lactide/glycolide molar ratio of 3, 1.5 and 1, respectively. Reprinted with permission from [11.32]

sules (Fig. 11.6) [11.36]. In interfacial polymerization, a monomer is dissolved in the emulsified nanodroplets and a second monomer (comonomer) is dissolved in the continuous phase. The two monomers undergo polymerization at the oil/water interface on the surface of the nanodroplets to form nanocapsules [11.36]. For example, poly(alkylcyanoacrylate)-based nanocapsules are synthesized using the interfacial polymerization method [11.37]. The alkylcyanoacrylate monomer dissolved in the oil nanodroplets reacts with hydroxyl ions in water and undergo interfacial polymerization at the oil/water interface [11.37]. Polybutylcyanoacrylate nanocapsules prepared via the method of interfacial polymerization had diameters of less than 150 nm, and the nanocapsules were used for encapsulation of the D-cycloserine drug [11.38]. Poly(ethyl 2-cyanoacrylate) nanocapsules synthesized using interfacial polymerization had ≈ 150 nm size and the nanocapsules were used for encapsulation of insulin [11.39]. Nanocapsules encapsulating hydrophilic drugs were synthesized by inverse emulsion (water/oil) using a thiol-isocyanate interfacial polymerization [11.40].

Conventional radical polymerization suffers from poor control over the molecular weight and polydispersity of the polymer chains which significantly influences the uniformity of polymeric NPs synthesized using radical polymerization [11.36]. Therefore, living radical polymerization has recently been employed to synthesize NPs with narrow size distributions [11.41]. For example, styrene monomer underwent reversible addition and fragmentation transfer (RAFT) polymerization in poly(*N*-isopropylacrylamide-*b*-dimethylacrylamide) based emulsions to form polystyrene NPs [11.42]. The resulting polystyrene NPs had 38–110 nm diameter and < 0.13 polydispersity index (derived from the standard deviation

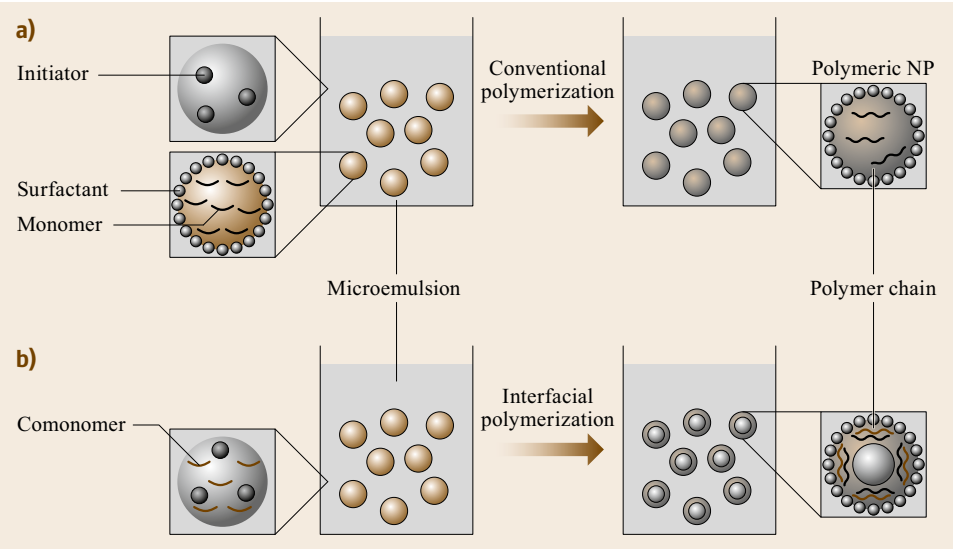

Fig. 11.6a,b Schematic representation of **(a)** conventional and **(b)** interfacial microemulsion polymerization

of the hypothetical Gaussian distribution) [11.42]. Nitroxide mediated polymerization (NMP), a well-known living polymerization technique, was employed to synthesize polystyrene, poly(*n*-butyl acrylate) or poly(methyl methacrylate) NPs with narrow size distributions [11.43–45]. Further, NPs based on poly(methyl methacrylate), poly(*n*-butyl methacrylate) and poly(ethylene oxide) were synthesized using the method of atom transfer radical polymerization (ATRP) [11.46–48].

In the nanoprecipitation method, the polymer is first dissolved in a water-miscible organic solvent. The polymer solution is then injected into a stirred aqueous solution containing a stabilizer (Fig. 11.3b). The spontaneous nanodrop formation followed by rapid diffusion of the organic solvent to the aqueous phase leads to polymer precipitation at the nanoscale and the formation of NPs stabilized by the stabilizer [11.36] (Fig. 11.3b). After NP formation, the organic solvent is removed by evaporation and the NPs are collected via centrifugation. The organic solvent in the nanoprecipitation technique should dissolve the polymer, be soluble in water, and have a low boiling point to facilitate its removal by evaporation. To satisfy the aforementioned criteria, acetone and tetrahydrofuran (THF) are widely used as solvents for nanoprecipitation [11.49, 50]. NPs of different polymers including PLA [11.50, 51], PLGA [11.49, 52], PCL [11.53, 54] and gelatin [11.55] were synthesized using the nanoprecipitation technique.

The dialysis method for the synthesis of NPs is based on solvent displacement similar to the nanoprecipitation method with the difference that there is a membrane barrier between the two phases in the dialysis method. In a typical procedure for the dialysis method, the polymer is dissolved in a water-miscible organic solvent, the organic solution is placed in a dialysis tube and dialyzed against distilled water [11.32]. The molecular weight cut off of the dialysis tube is usually smaller than the molecular weight of the polymer molecules but significantly larger than the solvents molecular weight. Therefore, the solvent diffuses out and water diffuses inside the dialysis tube while polymer molecules stay in the tube during dialysis. The solvent quality for the polymer in the dialysis tube decreases with time which causes polymer aggregation and precipitation at the nanoscale [11.24]. The formed NPs are stabilized by either a stabilizer or a hydrophilic block on the polymer molecule.

In the method of rapid expansion of a supercritical solution, the polymer is dissolved in a supercritical fluid (e.g., carbon dioxide) at high pressure and then the solution is expanded through an orifice or a nozzle into ambient air or a liquid. NPs are formed in the expansion jet due to a rapid pressure reduction [11.36]. The expansion of the supercritical solution into a liquid leads to the formation of uniform nanosized particles as opposed to expansion into air wherein both nanosized and microsized particles form [11.36]. For example, tetrahydrocurcumin (THC) loaded PLA NPs with 80−110 nm size and spherical morphology were synthesized by rapid expansion of supercritical solution of PLA and THC into water [11.56]. Further, NPs made of pure hydrophobic drugs including Naproxen and Ibuprofen have been synthesized using the rapid expansion of the supercritical solution technique [11.57, 58].

Organic–Inorganic Hybrid NPs

Hybrid NPs are composed of both organic and inorganic materials. The inorganic part may form the core or the shell of the hybrid NPs. Here, the methods for synthesis of hybrid NPs with inorganic core are discussed first followed by the discussion for the synthesis of hybrid NPs with organic core.

Hybrid NPs with Inorganic Core. Polymers can be grafted to the surface of inorganic NPs through covalent or noncovalent bonds (Fig. 11.7). Non-covalent attachment usually employs the electrostatic interaction between a charged polymer and an oppositely charged inorganic NP (Fig. 11.7a) [11.59]. For example, positively charged poly(allylamine hydrochloride) polymer was deposited on the negatively charged citrate-coated gold NPs using a layer-by-layer approach [11.60]. In another example, positively charged Fe_3O_4 NPs with 5 nm diameter were coated with negatively charged poly(acrylic acid)-*b*-poly(ethylene oxide) polymer. The coated NPs interacted with oppositely charged pristine NPs and formed aggregates with hydrodynamic diameter ranging from 50 to 100 nm [11.61].

The functional groups present on the surface of inorganic NPs (e.g., hydroxyl groups on the surface of metal oxide NPs) can be used to conjugate polymer chains to NPs (Fig. 11.7b) [11.62]. For example, polymethacrylic acid (PMAA) was conjugated to the surface of ZnO NPs through the reaction of −OH groups on the NP surface with carboxyl groups of PMAA [11.63]. In order to improve dispersion properties of silica NPs, poly(ethylene glycol) methacrylate (PEGMA) or poly(propylene glycol) methacrylate (PPGMA) were conjugated on the surface of vinyl-functionalized silica NPs via UV photo-polymerization [11.63]. Polystyrene was conjugated to TiO_2 NPs via a three-step process [11.64]. First, the surface of TiO_2 NPs was functionalized with phosphonic acid. Next, the surface of phosphonic acid modified NPs was functionalized with azide groups. Then, polystyrene was conjugated to azide functionalized NPs via the click reaction [11.64]. In another study, amine-terminated silica-coated Fe_3O_4 NPs were synthesized via sol-gel method and functionalized with alkyne groups using Michael addition of propargyl acrylate [11.65]. Then, poly(ester amine) was grafted to the alkyne-functionalized NPs using the click reaction [11.65].

In addition to grafting of preformed polymers to inorganic NPs, in situ polymerization of monomers on the surface of NPs (grafting from the surface) has been used extensively for the synthesis of organic–inorganic hybrid NPs (Fig. 11.7c) [11.66]. For example, densely grafted polystyrene and PMMA chains were grown on the surface of silica NPs by incorporation of atom transfer radical polymerization (ATRP) initiator on the surface of NPs [11.67]. A technique similar to ATRP was

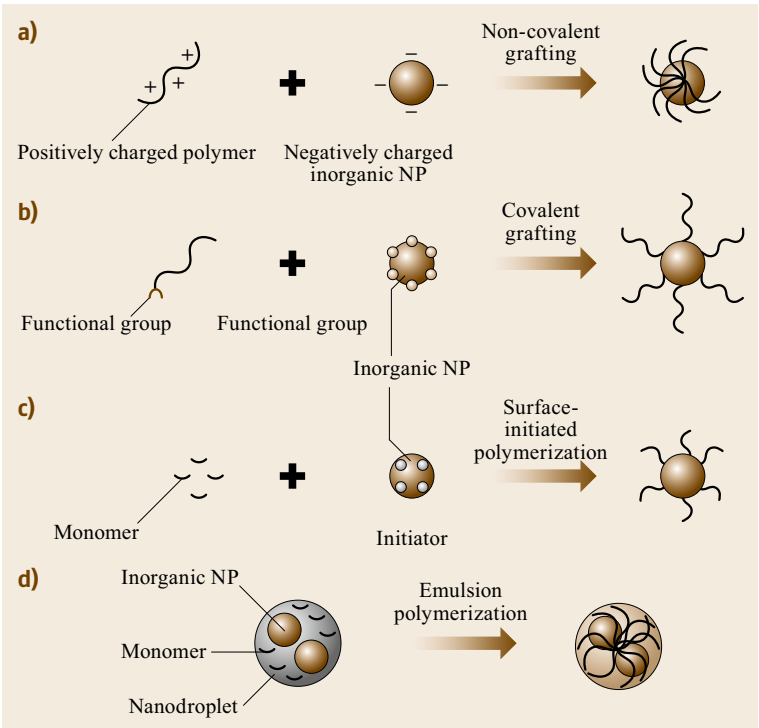

Fig. 11.7a–d Schematic representation of methods for the synthesis of hybrid NPs with inorganic core. **(a)** Non-covalent grafting of polymer chains to inorganic NPs via electrostatic complexation. **(b)** Covalent grafting of polymer chains to functionalized inorganic NPs. **(c)** Surface-initiated polymerization of monomers on inorganic NPs. **(d)** Emulsion polymerization of monomers in the presence of inorganic NPs

recently applied for the synthesis of PMMA-Al_2O_3 hybrid NPs [11.68]. In an attempt to synthesize thermoresponsive NPs, poly(*N*-isopropylacrylamide) (PNIPAm) chains were grown on the surface of Fe_3O_4 NPs using surface-initiated reversible addition-fragmentation transfer (RAFT) reaction [11.69]. The hydrodynamic diameter of the thermoresponsive hybrid NPs decreased from 37 to 24 nm when temperature increased from 28 to 36 °C [11.69]. PMMA-Fe_3O_4 hybrid NPs were synthesized using a thiol-lactam initiated radical polymerization technique [11.66].

Hybrid NPs can also be synthesized via emulsion polymerization of monomers in the presence of inorganic NPs (Fig. 11.7d). The surface of inorganic NPs is typically modified to increase compatibility with the polymer matrix [11.70]. For example, silica NPs with 20 or 78 nm diameter and hydrophobically-modified with γ-methacryloxypropyl trimethoxysilane (γ-MPS) were encapsulated in poly(methyl methacrylate-co-butyl acrylate) polymer NPs via emulsion polymerization [11.71]. Untreated silica NPs aggregated in the miniemulsion system and did not uniformly distribute in the poly(methyl methacrylate-co-butyl acrylate) NPs [11.71]. Polystyrene-silica hybrid NPs were synthesized via a miniemulsion polymerization technique using octaphenyl polyoxyethylene as a surfactant [11.72]. The hybrid polystyrene-silica NPs had a raspberry-like morphology with 130–370 nm diameter and 17–31% inorganic silica content [11.72]. Hybrid NPs with an inorganic TiO_2 core and organic polyacrylic shell were synthesized via emulsion polymerization of methyl methacrylate-butyl acrylate (inner shell) and dimethylaminoethyl methacrylate-butyl acrylate-acrylic acid (outer shell) in the presence of TiO_2 NPs modified with glycidyl methacrylate [11.73]. The TiO_2-polyacrylic hybrid NPs had 85–125 nm diameter [11.73]. Polystyrene nodules were formed on the surface of silica NPs via emulsion polymerization of styrene in the presence of silica NPs modified with an oxyethylene-based macromonomer [11.74]. The morphology of silica-polystyrene hybrid NPs depended on the ratio between silica seeds and growing polystyrene nodules and changed from snowman-like to daisy-like and raspberry-like morphology when increasing the ratio [11.74].

Hybrid NPs with Organic Core. Preformed inorganic NPs can be positioned on the surface of organic NPs using surface treatment followed by aggregation of inorganic–organic NPs (hetero-coagulation) (Fig. 11.8a) [11.70]. For example, negatively charged inorganic gold or silica NPs were deposited on the surface of polystyrene NPs functionalized with positively charged amine groups [11.75]. The position of inorganic NPs within the polymeric NPs can be adjusted by proper surface treatment. For example, gold NPs modified with mercaptoundecanol and dodecanethiol ligands were positioned in the shell of polystyrene-*b*-poly(acrylic acid) NPs whereas gold NPs modified with only hydrophobic dodecanethiol were distributed

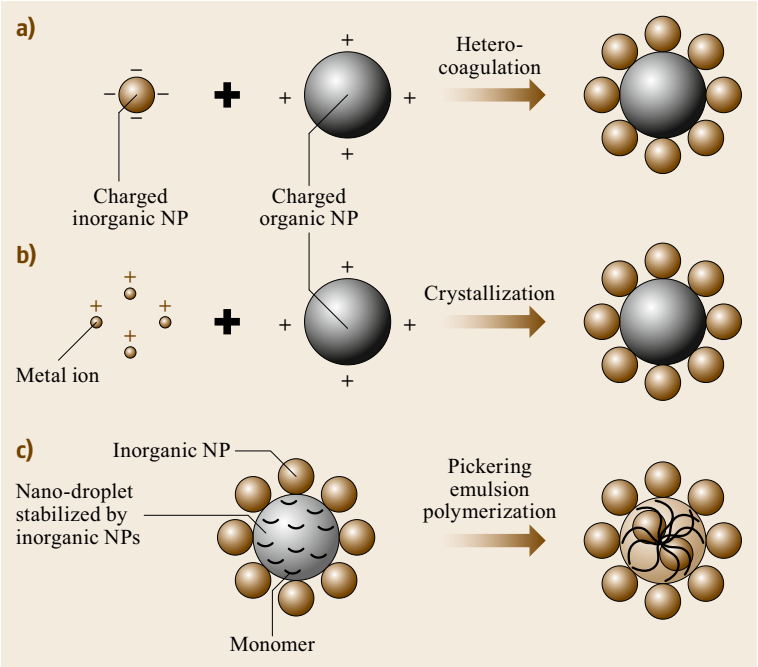

Fig. 11.8a–c Schematic representation of methods for the synthesis of hybrid NPs with organic core. **(a)** Hetero-coagulation of preformed inorganic and organic NPs. **(b)** Crystallization of inorganic NPs on the surface of organic NPs. **(c)** Pickering emulsion polymerization of monomers in the nanodroplets stabilized by inorganic NPs

in the core of the block-copolymer NPs [11.76]. Further, inorganic NPs can be covalently attached to the surface of organic NPs by conjugation. For instance, in an attempt to prepare fluorescent thermosensitive hybrid NPs, organic PNIPAM NPs were covered with inorganic CdTe nanocrystals via an amide coupling agent [11.77]. The photoluminescence (PL) intensity of the hybrid PNIPAM-CdTe NPs was temperature dependent [11.77].

Another approach for the synthesis of hybrid NPs is crystallization of inorganic materials on the surface of polymeric NPs (Fig. 11.8b) [11.70]. In this approach, the surface of polymeric particles should be charged to induce nucleation of the inorganic metals or metal oxides on the polymeric surface.

Several techniques including noncovalent assembly of a polyelectrolyte, covalent conjugation of a polyelectrolyte, and incorporation of a functional comonomer have been used to modify the surface of organic NPs for the synthesis of hybrid NPs [11.70]. For example, gold and platinum NPs (2–3 nm) were formed on the surface of polystyrene NPs (≈ 100 nm) covered with cationic 2-aminoethylmethacrylate polyelectrolytes [11.78]. In another example, styrene and a surface active comonomer (surfmer) with negatively charged phosphate groups underwent miniemulsion polymerization to form polystyrene NPs [11.79]. Negatively charged polystyrene NPs were then used for controlled crystallization of cerium, iron, and zinc oxide nanocrystals in aqueous or alcohol medium [11.79]. In addition, poly(styrene-co-acrylic acid) NPs surface-functionalized with negatively charged carboxyl groups were prepared via the miniemulsion technique and then covered with inorganic hydroxyapatite nanocrystals [11.80]. Calcium phosphate (CaP) NPs were deposited on the surface of PLA and PLGA nanofibers functionalized with negatively charged Glu-Glu-Gly-Gly-Cys peptide in a modified simulated body fluid (mSBF) (Fig. 11.9) [11.81, 82]. The deposition of CaP NPs increased and the size of NPs decreased when a carboxylate-rich organic acid such as citric acid, hydroxycitric acid, tartaric acid, malic acid, ascorbic acid, or salicylic acid was added to mSBF [11.81].

Hybrid NPs can also be synthesized via particle-stabilized emulsion polymerization (Pickering emulsion polymerization) technique (Fig. 11.8c). In Pickering emulsion polymerization, the surfactants are replaced with particle stabilizers [11.83]. Inorganic NPs used in the Pickering emulsion polymerization need to be wettable by both phases in the emulsion, be dispersible in the continuous phase and be able to accumulate at the interface of two phases [11.83]. The most widely used inorganic NPs as Pickering stabilizers are silica NPs [11.83]. For example, hybrid

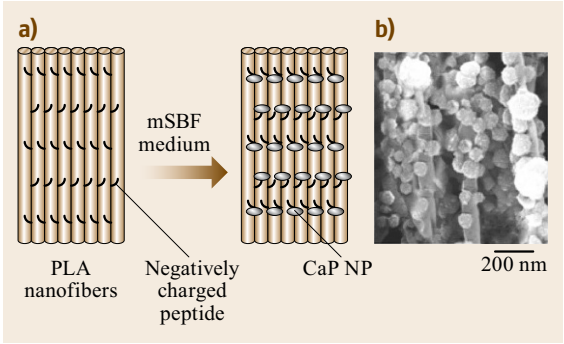

Fig. 11.9 **(a)** Schematic representation of the synthesis of CaP NPs on the surface of peptide functionalized PLA nanofibers. **(b)** SEM image of CaP NPs crystallized on the surface of peptide functionalized PLA nanofibers. Reproduced with permission from [11.81]

NPs were synthesized via Pickering emulsion polymerization of styrene, methyl methacrylate, *n*-butyl acrylate, or *n*-butyl methacrylate as a monomer and 4-vinylpyridine as a comonomer in the presence of silica NPs [11.84]. It was shown that a strong acid-base interaction between the copolymer and silica NPs is essential for the formation of hybrid NPs and hybrid NPs did not form in the absence of 4-vinylpyridine comonomer [11.84]. Silica-polystyrene hybrid NPs were synthesized via Pickering emulsion polymerization of styrene using a cationic azobisisobutyronitrile initiator (AIBN), glycerol functionalized silica and without using any comonomer [11.85]. The hybrid NPs had 200–400 nm diameter and 22–28 wt% silica [11.85]. In addition to silica, zinc oxide, titania, magnetite and graphene oxide NPs have been used as inorganic Pickering stabilizers in the synthesis of hybrid NPs [11.83]. For instance, ZnO-polystyrene hybrid NPs were prepared via emulsion polymerization of styrene in the presence of ZnO particles using AIBN as the initiator. The polystyrene formed the core while ZnO particles were positioned in the shell of the hybrid NPs [11.86].

Biological NPs

Biological NPs can be classified into two categories: Those that are naturally formed in biological systems from organic or inorganic materials (naturally occurring NPs) and those that are synthesized from biomolecules (e.g., proteins, peptides and polysaccharides).

Naturally Occurring NPs. Naturally occurring NPs are assembled in biological systems and include extracellular NPs (e.g., lipoproteins and viruses) and intracellular NPs (e.g., ferritin). Lipoproteins are self-assembled naturally occurring NPs made of lipids

and specialized proteins. Lipoproteins have a micellar structure with a core composed of triglycerides and cholesterol esters and a shell of phospholipids and amphipathic proteins [11.87, 88]. Lipoproteins are synthesized mainly by the liver and intestines and can be separated from plasma via ultracentrifugation [11.87, 88]. There are several classes of lipoproteins depending on size and density. The size of lipoproteins increases from 7–13 nm for high density lipoprotein (HDL) to 22–27 nm for low density lipoprotein (LDL), 27–30 nm for intermediate density lipoprotein (IDL), 35–80 nm for very low density lipoprotein (VLDL) and 80–1200 nm for chylomicrons [11.88]. Hydrophobic core of the lipoproteins can be loaded with water insoluble drugs for therapeutic applications. For example, valrubicin, an anticancer drug, was encapsulated in spherical HDL NPs [11.89]. The toxicity of valrubicin drug against ovarian and prostate cancer cell lines increased while its toxicity against normal prostate and ovarian epithelial cell lines decreased when the drug was encapsulated in HDL NPs compared with the drug alone [11.89].

Exosomes are 30–120 nm vesicles released by B cells, dendritic cells, mast cells, mesenchymal stem cells, adipocytes, neurons, endothelial cells and cancer cells in vivo [11.87, 90]. Further, exosomes are secreted by most cells in vitro [11.87]. In addition, exosomes can be isolated from extracellular fluids including blood, urine, saliva, and amniotic fluid [11.90]. The outer surface of exosomes is a lipid bilayer made of cholesterol, sphingolipids, ceramide and phosphoglycerides with saturated fatty-acyl chains [11.87]. The functions of exosomes in vivo include encapsulation and removal of excess membrane proteins and nucleotides from cells, encapsulation and delivery of signaling proteins and regulation of immune response through antigen presentation [11.91–93]. Proteins and nucleotides encapsulated in exosomes are protected from degradation and endocytosis by macrophages hence having a long circulation time [11.87]. Therefore, exosomes have been studied for the delivery of proteins and RNA in cancer treatment and tissue regeneration [11.90, 94].

Ferritin is an intracellular hollow nanoparticle with an outer diameter of 12 nm and interior cavity diameter of 8 nm [11.87]. Ferritin protein shell is composed of 24 subunits made up of the heavy-chain ferritin and the light-chain ferritin [11.87]. The interior cavity is naturally used to store iron oxides and to sequester the undesirable effects of iron ions. Ferritin NPs have been used as nanoreactors to synthesize ferrimagnetic iron oxide NPs in a constrained volume [11.95]. After the formation of inorganic core in the ferritin cavity, the protein shell can be removed to separate the inorganic NPs. In addition to iron oxide, inorganic cobalt oxide, chromium oxide and nickel hydroxide NPs have been synthesized in the cavity of ferritin NPs [11.96]. Further, semiconductor NPs including CdSe, ZnSe, CdS and ZnS NPs have been synthesized using ferritin [11.96]. It is shown that ferritin-iron oxide hybrid NPs bind to tumor cells that overexpress transferrin receptor 1 (TfR1) and undergo a color reaction that can be used to visualize tumor tissues [11.97].

Viruses are naturally occurring NPs (20–300 nm) with capsid proteins forming the shell and viral DNA or RNA forming the core [11.87]. Viruses have a wide range of sizes and morphologies including spherical, rod-shape, and icosahedral morphologies [11.87]. Virus-like particles with a native protein shell but without nucleic acid do not cause infection and can be used as carriers for drugs or proteins. Further, bioactive ligands can be conjugated to lysine or cysteine residues on the capsid protein [11.98]. For example, cell penetrating peptides conjugated to Cowpea mosaic virus (CPMV) increased the uptake efficiency of the virus by human cervical cancer cells [11.99]. In another example, conjugation of nucleoprotein of influenza to Bacteriophage P22 virus-like particles resulted in a vaccine that induced a protective $CD8^+$ T cell response against lethal doses of influenza while the virus-like particles alone did not provide immunity [11.100].

Protein NPs. Several techniques including desolvation, emulsion–solvent extraction and polyelectrolyte complexation have been employed for the synthesis of NPs from proteins [11.101]. The desolvation method is based on drop-wise addition of a desolvation agent such as alcohols, salts or other solvents to a protein solution with stirring to trigger precipitation of protein NPs [11.102]. Since the solubility and conformation of proteins in aqueous solution depends on pH, solvent polarity, and ionic strength of the solution, a change in these factors leads to conformational changes and nanoprecipitation of proteins [11.101]. The precipitation step is often followed by crosslinking of NPs with glutaraldehyde in order to stabilize the particles [11.102]. NPs of different proteins including albumin, gelatin and elastin have been synthesized via the desolvation method [11.101]. For example, human serum albumin (HSA) NPs were prepared via the slow addition of ethanol to HSA solution at room temperature followed by glutaraldehyde crosslinking [11.103]. The size of HSA NPs varied between 200–300 nm depending on pH of the desolvation solution [11.103]. The size of the albumin NPs prepared via desolvation decreased with increasing pH and increasing the ratio of antisolvent (e.g., ethanol) to solvent [11.101, 103]. Bovine serum albumin (BSA) NPs synthesized via desolvation and surface modified with cationic polyethylenimine were

employed for the encapsulation of bone morphogenic protein-2 (BMP-2) protein [11.104]. The NPs exhibited a sustained release of BMP-2 over 10 days and high retention of protein activity in vitro [11.104]. In another example, gelatin NPs were synthesized by slow addition of ethanol to the aqueous solution of gelatin with 65 : 35 ethanol/water ratio at 37 °C and pH = 7.0 followed by particle crosslinking with glyoxal [11.105]. The gelatin NPs had a 17 h half-life and 30 h mean residence time in the plasma of Lewis lung carcinoma-bearing mice [11.105].

The emulsion–solvent extraction method for the synthesis of protein NPs is based on emulsification of the aqueous solution of the protein in oil using a high-speed homogenizer or a sonicator in the presence of a surfactant such as phosphatidylcholine or Span 80 [11.101]. The oil phase is then removed using an organic solvent and NPs are separated via centrifugation [11.101]. NPs can be stabilized using a physical or chemical crosslinking technique. For example, NPs based on casein, a milk protein, were synthesized via oil-in-water emulsification in the presence of Span 80 [11.106]. Casein NPs were stabilized via ionic crosslinking using a polyanionic crosslinker sodium tripolyphosphate [11.106]. Casein NPs had 60−100 nm diameter and exhibited a sustained release of anticancer drug flutamide for four days in vitro [11.106]. NPs based on albumin protein were also synthesized using the emulsion–solvent extraction method [11.101, 107].

Polyelectrolyte complexation is typically used for the synthesis of DNA-laden protein NPs [11.101]. In this method, proteins are first charged cationic by adjusting the pH to below their isoelectric point (pI) (Fig. 11.10). Cationic proteins then form a polyelectrolyte complex with negatively charged DNA that undergo desolvation to form DNA-laden NPs [11.101]. For example, HSA-DNA-polyethylenimine (PEI) NPs were synthesized in a two-step process [11.108]. First, a solution of PEI and positively charged HSA was prepared at pH 4.1. Then, NPs were formed by adding sodium sulfate solution containing DNA to the HSA-PEI solution [11.108]. Positively charged poly(lysine) and chitosan were also used for the synthesis of NPs via the polyelectrolyte complexation method [11.24].

Peptide NPs. Several classes of peptides including surfactant-like peptides and polypeptides have been used for the synthesis of NPs [11.109, 110]. The surfactant-like peptides have a hydrophilic head and a hydrophobic tail similar to an organic surfactant. The peptides self-assemble in aqueous solution to form micelles with different morphologies including nanotubes, nanovesicles and nanofibers [11.111]. For instance, surfactant-like peptides with a tail of six hydrophobic amino acids and a head of two positively charged amino acids (e.g., V_6K_2, V=Valine, K=Lysine) self-assembled to nanotubes and spherical nanovesicles in aqueous solution [11.112]. The V_6K_2 peptide conjugated to a low molecular weight PLA molecule (PLA-V6K2) was self-assembled to spherical NPs with an average size of 100 nm (Fig. 11.11a) [11.113]. The PLA-V6K2 NPs had sustained release of an anticancer drug Doxorubicin (Dox) over 35 days (Fig. 11.11b) [11.113]. Further, 49% of the PLA-V6K2 NPs were taken up by 4T1 mouse breast carcinoma cells after 24 h (Fig. 11.11c) [11.113]. The release rate of Dox was slower and the percent uptake by 4T1 cells was higher for PLA-V6K2 NPs compared with PEG stabilized PLA (PLA-EG) NPs (Fig. 11.11b,c) [11.113].

When the hydrophobic tail of a surfactant-like peptide is an alkyl chain, the structure is called peptide amphiphile (PA). It is shown that PAs spontaneously self-assemble into a range of nanostructures including nanofibers, spherical micelles, nanovesicles and nanotubes [11.114, 115]. For example, a PA with the structure of C_{16}-KKFFVLK (F= Phenylalanine, L= Leucine) self-assembled into nanotubes and helical ribbons at room temperature [11.116].

A number of polypeptides have been used for synthesis of NPs [11.117]. For example, an elastin-like polypeptide (ELP) with a repeating unit of VPAVG (P=Proline, A=Alanine, G=Glycine) self-assembled to NPs when the temperature of polypeptide aqueous solution was raised from 4 to 37 °C [11.118]. The elastin-like polypeptide NPs exhibited a sustained release of encapsulated dexamethasone phosphate for 30 days in vitro at 37 °C [11.118]. In a recent example, NPs with 600 nm diameter were synthesized from an ELP conjugated to stromal cell-derived growth factor-1 (SDF1) for wound healing applications [11.119]. The wounds of diabetic mice treated with ELP-SDF1 NPs were closed after 28 days while those wounds treated with SDF1 alone were closed after 42 days [11.119]. pH sensitive polypeptide nanovesicles were synthesized from zwitterionic diblock poly(L-glutamic acid)-*b*-poly(L-lysine) copolymers. The hydrodynamic radius of the nanovesicles was 110 and 175 nm in acidic (pH < 4) and basic (pH > 10) aqueous solutions while the polypeptides did not self-assemble to nanovesicles at intermediate pH values (5 < pH < 9) [11.120].

Polysaccharide NPs. Polysaccharides are naturally derived polymers with monosaccharide repeat units joined together by glycosidic bonds [11.110]. Positively charged chitosan and negatively charged alginate, heparin, hyaluronic acid, dextran sulfate and der-

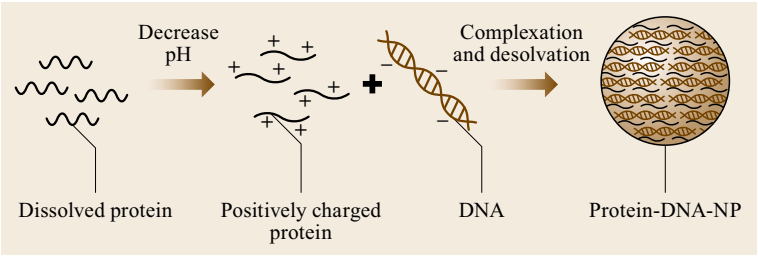

Fig. 11.10 Schematic representation of the polyelectrolyte complexation method for synthesis of protein–DNA NPs

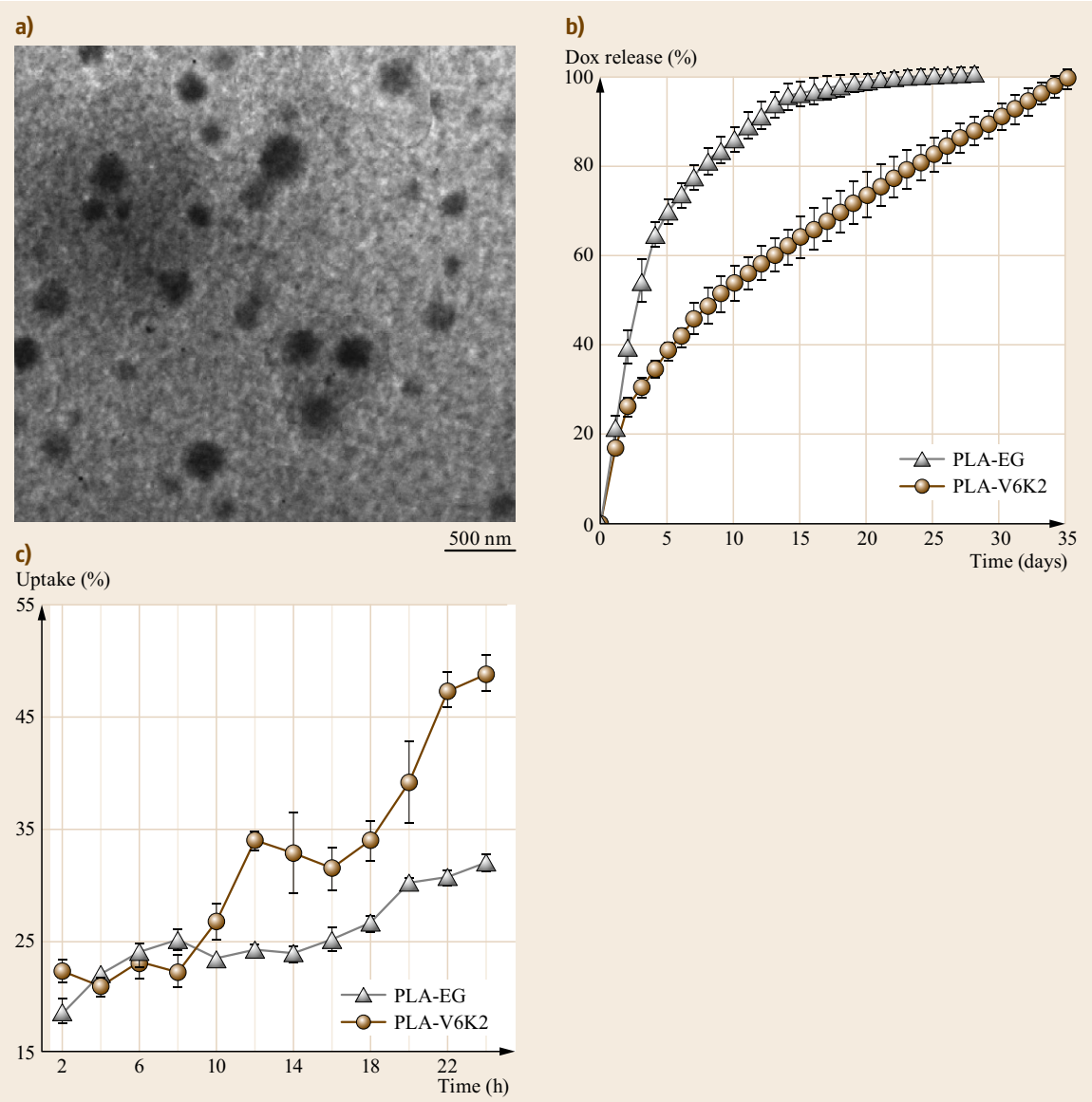

Fig. 11.11 **(a)** TEM image of the uranyl acetate stained PLA-V6K2 NPs. **(b)** Release profile of Dox encapsulated in PLA-V6K2 and PLA-EG NPs incubated in PBS. **(c)** The effect of incubation time on percent uptake of PLA-V6K2 and PLA-EG NPs by 4T1 breast tumor cells. Reprinted with permission from [11.113]

matan sulfate are the most widely used polysaccharides for synthesis of NPs [11.110]. Different approaches including polyelectrolyte complexation, crosslinking, and self-assembly have been employed for the synthesis of polysaccharide NPs [11.110]. For example, chitosan-alginate NPs were prepared by polyelectrolyte complexation between cationic chitosan and anionic alginate pregel particles [11.121]. Polysaccharide NPs prepared by polyelectrolyte complexation between dermatan and chitosan had 730 nm radius and were selectively taken up by H5V murine endothelial cells in the presence of Raw 264.7 murine macrophage cells [11.122]. Chitosan NPs (250 nm diameter) synthesized via water-in-oil emulsion method, stabilized by glutaraldehyde crosslinking, and coated with anionic polysaccharides were used for encapsulation of the anticancer drug 5-fluorouracil (5-FU) [11.123]. Self-assembling amphiphilic polysaccharides generated by hydrophobic modification of polysaccharides' backbone have also been used for the synthesis of NPs and micelles [11.110]. For instance, hydrophobically modified chitosan prepared via grafting *N*-acyl groups to the backbone of chitosan self-assembled to NPs with < 550 nm diameter at 38 °C and pH 7.4 [11.124]. In another example, polyglycolic acid (PGA) conjugated alginate self-assembled to NPs with 200–250 nm diameter through hydrophobic interactions between the PGA segments [11.125].

11.3 Properties of NPs

11.3.1 Size of NPs

A change in NP size significantly affects the surface area as well as mechanical, magnetic, electrical and biological properties of NPs. The surface to volume ratio increases when the particle size decreases. Therefore, the fraction of surface atoms or functional groups increases with decreasing the NP size. For example, the chemical reactivity of silica NPs increases with decreasing the particle size due to an increase in the density of silanol groups (Si–OH) on the NPs surface [11.126]. The superparamagnetism of magnetic NPs increases as the size decreases [11.127]. The elastic modulus and hardness of crystalline metal NPs is inversely correlated with particle size [11.95]. The capacitance of conductive NPs decreases and Coulomb energy increases with reducing the NP size [11.128]. Anticancer drug-loaded NPs with diameters < 100 nm can pass through the leaky vasculature of the tumor tissues [11.129]. The size of NPs can be controlled by adjusting the synthesis parameters including reactant–surfactant concentration, temperature and pH of the medium [11.12].

In the ball milling method, the size of synthesized NPs depends on milling time, rotation speed, ball-to-powder weight ratio as well as temperature and pressure [11.1]. The size of NPs synthesized via the vapor deposition method depends on target to substrate distance, type of substrate, substrate temperature, deposition time, chamber pressure and the electrical power for deposition [11.6]. In the laser-based vapor deposition method, number of pulses, deposition time, gas pressure and substrate temperature significantly affects the size and morphology of NPs [11.7, 8] The size of NPs synthesized via reduction and precipitation methods can be controlled by changing pH of the synthesis medium. The adsorption of proton or hydroxide ions on the surface of growing particles decreases the surface energy of growing NPs, hence increases the stability of small particles [11.130]. Therefore, adjusting pH of the synthesis medium to values that increase the surface charge density of growing particles decreases the size of NPs [11.130]. For instance, in the synthesis of TiO_2 NPs via precipitation method, the surface charge density increased from 0 to 0.2 and the size of NPs decreased from 9 to 5 nm by decreasing pH of the synthesis medium from 5.3 to 2 [11.14].

In the microemulsion method, NPs of smaller size can be synthesized by reducing water to surfactant ratio. An increase in the water to surfactant ratio, increases the droplet size as well as the aggregation of particles, hence increases size of the synthesized NPs. For example, Pd NPs were synthesized via the microemulsion technique in a water/isooctane medium using sodium bis(2-ethylhexyl) sulfosuccinate as the surfactant and N_2H_4 as the reducing agent [11.131]. The size of Pd NPs after 10 min of reaction increased from 8.1 to 11.7 nm with increasing the water to surfactant ratio from 3 to 7 at reducing agent to metal molar ratio of 60 [11.131]. In another example, a higher concentration of PVA stabilizer in the single-emulsion synthesis of PLGA polymer NPs decreased the size of particles significantly [11.132]. Further, the size of NPs in the microemulsion technique can be reduced by using a more viscous oil phase [11.133]. In addition, high-energy mixing (e.g., sonication) of microemulsion systems decreases the size of synthesized NPs [11.12]. An increase in the concentration of the reactants in the microemulsion technique decreased the size of NPs which was due to a transition from intermicellar nucleation to intramicellar nucleation [11.134, 135].

The size of polymer NPs prepared via dialysis or nanoprecipitation depends on the polymer composition and concentration and the solvent used. The size of nanoprecipitated NPs decreases with increasing solvent–nonsolvent affinity as well as polymer-solvent affinity [11.136]. For example, the size of PLGA NPs decreased with changing the solvent from dimethylacetamide (DMAc) to dimethylsulfoxide (DMSO) and dimethylformamide (DMF) in the dialysis method [11.137]. In another example, the size of poly(lactide-*co*-glycolide fumarate) (PLGF) NPs synthesized by the dialysis method was smaller than poly(lactide fumarate) (PLAF) NPs due to the higher hydrophilicity of the PLGF macromer [11.138].

11.3.2 Shape of NPs

The shape of NPs significantly affects their physicochemical and biological properties. For example, the catalytic activity of Pt NPs is shape dependent [11.139] or the circulation time and cell uptake of drug-loaded NPs varies with the NPs' morphology [11.140]. NPs generally favor a morphology that is associated with minimal surface free energy [11.15]. For amorphous materials with an isotropic surface, a spherical morphology minimizes the surface free energy by lowering the surface to volume ratio [11.15]. In an anisotropic crystalline structure, each crystal plane has a specific surface free energy [11.130]. For example, in noble metals (e.g., Ag, Au and Pt), the surface free energy of (100), (110) and (111) planes is lower than those of high-index crystal planes. Therefore, the standard morphology of NPs made of single crystalline noble metals is a truncated octahedron that is a linear combination of the aforementioned low-index planes [11.15]. However, the shape of crystalline metal or metal oxide NPs synthesized via solution-based methods can be modified by adjusting the nucleation and growth steps. For example, the shape uniformity of NPs increases by increasing the rate of crystal nucleation in the salt reduction method [11.15]. Further, adsorbates that selectively adsorb to specific crystal planes in the growth step can be employed to control the crystal morphology [11.15]. The crystal growth continues on the plane that has weak interaction with the adsorbate. Surfactants, poly(vinyl pyrrolidone) and metal ions have been used as adsorbates in the synthesis of crystalline NPs [11.15]. For instance, single crystalline Ag NPs with several morphologies including cube, octahedral, truncated cube, truncated octahedra and cuboctahedra were synthesized via reduction of $AgNO_3$ in 1,5-pentanediol in the presence of poly(vinyl pyrrolidone) as an adsorbate at 180 °C [11.141]. The morphology of Ag NPs depended on the rate of injection of $AgNO_3$ solution in the reducing solvent [11.141]. The morphology of inorganic NPs can also be controlled by adjusting the reaction parameters such as temperature, pH and relative concentration of metal ions. For example, manganese dioxide (MnO_2) NPs with a number of morphologies including needle-like, lamellar and spherical were synthesized by varying the Mn(VII) to Mn(II) ratio and pH of the reducing medium [11.130].

Due to the semicrystalline nature of polymers, the favorable morphology of polymeric NPs is spherical [11.142]. Polymeric NPs with nonspherical morphologies have been synthesized via top-down and bottom-up approaches. For example, several morphologies of polystyrene NPs including ellipsoids, rods and disks were synthesized by embedding the spherical polystyrene NPs in a poly(vinyl alcohol) film and stretching the film [11.143]. Further, several morphologies of polyethylene glycol (PEG) based NPs including spheres, cylinders, cubes and disks were synthesized via spraying or drop-casting the polymer precursor solution on a perfluoropolyether nonwetting template [11.144]. Polymer and peptide based NPs with a range of morphologies have been synthesized via the self-assembly method. For example, worm-like micelles were synthesized via self-assembly of poly(ethylene glycol)-poly(ethylethylene) diblock copolymers [11.145]. Surfactant-like peptides with a tail of six hydrophobic amino acids and a head of two positively charged amino acids (e.g., V_6K_2) self-assembled to nanotubes and spherical nanovesicles in aqueous solution [11.112]. Furthermore, it was shown that peptide amphiphiles spontaneously self-assemble into a variety of nano-objects including spherical micelles, nanovesicles and nanotubes [11.114, 115].

11.3.3 Magnetic Properties of NPs

Magnetic NPs have been synthesized with several compositions including iron oxides, pure metals, alloys (e.g., FePt) and spinel-type compounds (e.g., $MnFe_2O_4$ or $CoFe_2O_4$) [11.146]. Further, a number of approaches including coprecipitation, microemulsion, thermal decomposition and hydrothermal synthesis have been applied for the synthesis of magnetic NPs [11.146]. The majority of magnetic NPs are classified into either ferromagnetic or superparamagnetic materials [11.127]. In ferromagnetic materials, atomic magnetic dipoles are aligned and there exists a net magnetic moment in the absence of an external magnetic field. Paramagnetic materials have magnetic dipoles but these dipoles are not aligned and fluctuate randomly, hence the net magnetic moment is zero in the absence of an external magnetic field above a material-specific temperature called the Curie temperature. Ferromagnetic or fer-

rimagnetic NPs with sizes below a material-specific threshold have zero net magnetic moment in the absence of an external field and they become magnetic and their magnetic moment rapidly increases with the application of an external magnetic field (Fig. 11.12). This property of magnetic NPs which is called superparamagnetism occurs at temperatures above a blocking temperature (T_B) wherein thermal fluctuations exceed the energy barrier for random flipping of magnetic moments within NPs [11.127].

The T_B of NPs correlates with particle volume and rapidly increases with particle diameter [11.148]. The maximum on the magnetization curve (Fig. 11.12) is called saturation magnetization (M_s) which happens when all magnetic dipoles are aligned with the external magnetic field [11.127, 147]. The remaining magnetization after the removal of an external magnetic field (the intercept of y-axis and the magnetization curve in Fig. 11.12) is called remanent magnetization (M_r) [11.147]. The strength of an external field required to force the magnetization to zero (the intercept of x-axis and the magnetization curve in Fig. 11.12) is called coercivity (H_c) [11.147]. The M_r and H_c are both zero for paramagnetic and superparamagnetic materials as opposed to ferromagnetic materials (Fig. 11.12) [11.147]. The magnetization of superparamagnetic materials increases rapidly upon applying an external field as opposed to the linear trend of paramagnetic materials (Fig. 11.12) [11.147]. The M_s increases linearly with NP size and reaches a plateau corresponding to the bulk M_s [11.127]. Therefore, smaller NPs have lower M_s but higher superparamagnetism. For example the M_s of $Fe_{2.66}O_4$ NPs decreased from 77 to 29 emu/g and T_B decreased from 100 to 10 K when the NP size was reduced from 14 to 2.5 nm [11.149]. In addition to size, the morphology of NPs affects magnetization. For example, the T_B of Fe_3O_4 NPs decreased when the NPs morphology was changed from spherical to cubic [11.150]. Further, the M_s of Fe_3O_4 NPs increased from 18 to 40 and 80 emu/g when the NPs morphology was changed from rods to cubes and spheres, respectively [11.107]. The composition and method of synthesis of NPs also significantly affects magnetic properties of NPs. For instance, the size at which a transition to superparamagnetism happens decreased when the composition of NPs was changed from Fe_2O_3 to Fe_3O_4 and FePt [11.151]. Alloyed magnetic NPs generally have higher M_s than the corresponding pure metals or iron oxide based NPs [11.127]. In another example, metal-doped NPs with the composition of MFe_2O_4 (M = Mn, Fe, Co or Ni) were synthesized via a nonhydrolytic reaction between iron tris-2,4-pentadionate and divalent metal chloride (MCl_2). The M_s of MFe_2O_4 NPs with the same size of 12 nm varied from 85 to 99, 101 and 110 emu/g by changing the metal (M) from Ni to Co, Fe and Mn, respectively [11.152]. The highest M_s of $MnFe_2O_4$ was related to a mixed spinel structure as opposed to an inverse structure for $NiFe_2O_4$, $CoFe_2O_4$ and $FeFe_2O_4$ NPs [11.152]. Particle coating generally decreases the magnetization of NPs [11.127]. For example, M_s of Fe_3O_4 NPs decreased from 75 to 51 emu/g and coercivity increased from 1.1 to 5 when the NPs were coated with PNIPAM polymer [11.153].

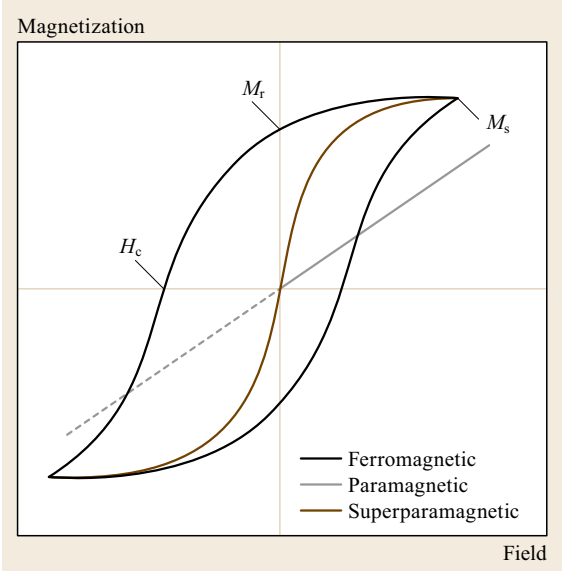

Fig. 11.12 Hysteresis loops of ferromagnetic, paramagnetic, and superparamagnetic materials (after [11.147])

11.3.4 Mechanical Properties of NPs

The mechanical properties of NPs including elastic modulus, hardness, and frication are significantly different from those of bulk materials [11.154]. Results of several studies have shown that the hardness, yield strength, and elastic modulus of crystalline metal NPs are higher than those of bulk metals and inversely correlated with particle size [11.155–158]. For example, the mechanical properties of gold NPs with a sixfold icosahedral symmetry and 22 nm size were measured via the nano-indentation method [11.157]. The hardness and elastic modulus of gold NPs were 1.72 and 100 GPa, respectively, which were significantly higher than the hardness (216 MPa) and elastic modulus (79 GPa) of gold [11.157]. The increase in yield strength or hardness with decreasing size for single crystalline NPs is due to the absence of dislocations in the crystalline structure leading to higher resistance to plastic deformation [11.154]. For polycrystalline NPs, the enhanced mechanical properties are due to an increase in the den-

sity and entanglement of dislocations with decreasing the grain size that limits the motion of dislocations (Hall–Petch effect) [11.159]. However, the hardness and yield strength of crystalline NPs decrease significantly if the NPs are smaller than a critical size due to the inverse Hall–Petch effect [11.154]. In this case, the grain is too small to support a high density of dislocations hence the deformation is dominated by grain boundary sliding [11.154]. For example, the modulus of nanocrystalline titania NPs increased with reducing the particle size down to 15 nm [11.160]. The modulus of titania NPs then decreased with decreasing particle size below 15 nm [11.160]. The mechanical properties of polymeric NPs depend on the glass transition temperature, crystallinity of the polymer as well as the surface properties of NPs [11.161]. For instance, the compressive modulus of surface-charged polystyrene NPs was slightly less than that of bulk polystyrene but the elastic modulus of polypropylene NPs was higher than that of bulk polypropylene [11.162, 163].

The friction coefficient of nano-objects is proportional to the contact area as opposed to the macroscopic dry sliding friction. Results of a number of studies showed that the friction of NPs increases with particle size [11.154, 161]. For example, an increase in the size of gold NPs from 30 to 90 nm, increased the dry friction of particles under 300 nN load by threefold [11.164]. Further, gold nanorods with 50 nm diameter and 200 nm length had a higher friction in air or water than gold NPs with 50 nm diameter [11.154]. The friction force between single polystyrene NPs (30–230 nm) and a silicon substrate was correlated with two thirds power of the particle radius [11.165]. Further, the frication of nano-objects increased logarithmically with the sliding velocity as opposed to the macroscopic frication which was independent of sliding velocity [11.166].

11.3.5 Electrical Properties of NPs

The semicontinuous electronic band structure of bulk metals changes to discrete electronic levels when decreasing the size in the nanoscale. This phenomenon is called the size quantization effect, which is responsible for the unique electrical properties of metallic and semiconductive NPs. A transition from a conductive bulk material to semiconductive NP happens due to the size quantization effect and formation of a band gap if the size of NP is sufficiently low. Metallic NPs with a diameter lower than 2 nm start to undergo transition from conductor to semiconductor [11.167]. Further, the band gap that normally exists in semiconductive materials grows with decreasing size from bulk to NPs. However, the quantization effect in semiconductor materials happens at relatively larger scales (1–10 nm) [11.167]. The electrical current in bulk materials obeys Ohm's law

$$V = IR\,, \tag{11.4}$$

where V is the applied voltage, I is current and R is resistance of the material. Ohm's law is not valid when quantization happens at the nanoscale and the Coulomb energy of NPs exceeds the thermal energy

$$k_{\mathrm{B}}T < \frac{e^2}{2C}\,, \tag{11.5}$$

where k_{B} is the Boltzmann constant, T is temperature, e is elementary charge and C is capacitance. The capacitance of a nanoparticle depends on its size as [11.128]

$$C = 4\pi r\varepsilon\varepsilon_0\,, \tag{11.6}$$

where r is the NP radius, ε and ε_0 are dielectric constant of the medium and vacuum, respectively. Therefore, capacitance decreases and Coulomb energy increases with reducing NPs size. When the NPs are sufficiently small such that Coulomb energy exceeds thermal energy (11.5), charge transfer occurs through the NPs via a single electron tunneling. In this case, the external voltage $\Delta V = e/2C$ is required to transfer a single charge to the NP leading to a tunneling current $\Delta I = e/RC$. Therefore, the current–voltage curve in quantum dots is like a staircase with height of ΔI and width of ΔV, due to tunneling of multiple single electrons [11.128]. For example, Au NPs with 5.8 nm diameter at 77 °K had a staircase current–voltage curve with a width of $\Delta V =$ 200 mV [11.168].

11.4 Applications of NPs

NPs have been used for sensing biological analytes including DNA and proteins as well as small molecules such as glucose [11.11]. In biosensing, specific receptors conjugated to the surface of NPs interact with specific biological analytes and the biological recognition event is translated into detectable optical, magnetic or electrochemical signals [11.169, 170]. The increased sensitivity and lower detection limit of NP-based biosensors compared with macroscale biosensors are due to high surface to volume ratio of NPs resulting in a larger density of biospecific receptors per unit volume of NPs [11.11]. Further, unique magnetic,

optical and electrical properties of NPs contribute to the translation of recognition event to detectable signals [11.11]. For example, Au NPs were used for colorimetric sensing of oligonucleotides [11.169]. Au NPs functionalized with single-stranded DNA aggregated in the presence of oligonucleotides leading to a change in the color of solution [11.169]. In another example, interleukin-6 (IL-6) protein in the unprocessed human sera was detected using IL-6 antibody conjugated magnetic FeCo NPs and a giant magnetoresistive (GMR) sensor functionalized with IL-6 antibody [11.171]. The IL-6 analyte and antibody-conjugated magnetic NPs were captured and formed a sandwich on the surface of the GMR sensor [11.171]. The change in electrical resistance of the GMR sensor was correlated to the amount of captured magnetic FeCo NPs, which was related to the concentration of IL-6 protein [11.171].

One of the major applications of NPs is the localized or targeted delivery of drugs and biomolecules to cells and tissues [11.172]. NPs as delivery vehicles protect drugs or biomolecules from degradation, transport them into the cells or tissues and release them in a sustained manner [11.169]. The uptake efficiency of bioactive molecules by cells is significantly higher for NPs compared with microparticles. For example, PLGA NPs (100 nm) had 15–250-fold higher gastrointestinal tissue uptake in a rat model than microparticles (10 μm) [11.173]. Anticancer-drug-loaded NPs with diameters < 100 nm can pass the leaky vasculature of tumors and enter the interstitial space of tumor tissue [11.129]. Several biodegradable NPs based on PLA, PLGA, PCL and polyacrylate polymers as well as natural alginate, chitosan and gelatin have been synthesized for the delivery of drugs or proteins [11.172]. The drug or protein may be entrapped within the NPs or conjugated on the surface of NPs. Further, targeting antibodies can be attached to the surface of NPs for recognition and binding to target cells [11.174]. The release rate of encapsulated drugs or proteins from biodegradable polymer NPs can be tuned from a few days to months by altering the composition or length of the polymer chains [11.172]. For example, anticancer drug Paclitaxel encapsulated in the more hydrophobic NPs based on poly(lactide-fumarate) (PLAF) displayed a sustained release of Paclitaxel over 28 days whereas the less hydrophobic poly(lactide-co-glycolide fumarate) (PLGF) NPs released the encapsulated drug in 15 days [11.175]. The viability of HCT116 human colon carcinoma cells significantly decreased when they were exposed to Paclitaxel encapsulated in PLGF or PLAF NPs compared with the drug alone [11.175]. In a recent example, recombinant human bone morphogenetic protein-2 (BMP2) and vascular endothelial growth factor (VEGF) were grafted to nanogels based on polyethylene glycol (PEG) macromers chain-extended with short lactide and glycolide segments [11.32]. The release rate of BMP2 and VEGF proteins from nanogels depended on PEG molecular weight, lactide/glycolide segment length and lactide–glycolide molar ratio in the polymer [11.32]. Nanogels with 12 kDa PEG molecular weight, 24 lactide-glycolide segment length, and 60 : 40 lactide/glycolide ratio released the grafted VEGF in 10 days and induced vasculogenic differentiation of human endothelial colony-forming cells while nanogels with 8 kDa PEG molecular weight, 26 lactide-glycolide segment length, and 60 : 40 lactide–glycolide ratio released the grafted BMP2 in 21 days and induced osteogenic differentiation of human mesenchymal stem cells [11.32].

Several types of NPs including noble metal NPs, quantum dots, polymer NPs and fluorescently doped silica NPs have been used for imaging of cells and tissues [11.176]. For example, self-illuminating quantum dots were synthesized by conjugation of a modified bioluminescent protein *Renilla reniformis* luciferase to fluorescent semiconductor CdSe/ZnS quantum dots [11.177]. The conjugate emitted long-wavelength bioluminescent light without a need for external excitation of quantum dots [11.177]. Further, magnetic NPs have been used as contrast agents in magnetic resonance imaging (MRI) [11.178]. MRI signal intensity is related to the spin–lattice relaxation time (T_1) and spin–spin relaxation time (T_2) of water protons [11.178]. When magnetic NPs accumulate in the tissue that is being imaged, they reduce the relaxation time which in turn enhance the image contrast [11.127]. The contrast enhancement is correlated with the M_s of the magnetic NPs [11.127]. For example, Fe_3O_4 NPs shorten the T_2 relaxation time and have been used as a contrast agent in imaging liver, spleen and bone marrow [11.179].

One of the earliest commercial applications of NPs was in catalyzed reactions such as the synthesis of reformulated gasoline and hydrosilylation reactions [11.180]. Metal NPs have been used as catalysts in quasihomogeneous catalyzed reactions including hydrogenation, cross-coupling, oxidation and electron transfer in organic or aqueous solutions [11.180]. For instance, hydrogenation of cyclooctene to cyclooctane was performed via quasihomogeneous catalysis using chitosan-stabilized Pt and Pd NPs (1.9–2.2 nm in size) as catalysts in acetic acid/methanol solution [11.181]. Further, metal NPs deposited on carbon, silica, and metal oxide supports have been used as catalysts in heterogeneous catalysis [11.180]. Several techniques including physical adsorption, grafting, flame spraying, ion exchange and the Langmuir–Blodgett method

have been employed for deposition of NPs on supports for heterogeneous catalysis [11.182–184]. The size, shape and composition of NPs significantly affect the catalytic properties of supported metal catalysts [11.180]. For example, Pt NPs of different shapes (cubic and cuboctahedral) deposited on silicon wafer supports via Langmuir–Blodgett technique were used for hydrogenation of benzene [11.183]. Selectivity of the heterogeneously catalyzed reaction depended significantly on the shape of Pt NPs. While cyclohexane and cyclohexene were formed on cuboctahedral NPs, only cyclohexane was formed on cubic NPs [11.183].

Metal, metal oxide, silicon and carbon-based NPs have been used as additives to lubricants in order to reduce the friction and wear between contacting surfaces [11.161]. The reduction of friction and wear in the presence of NPs is related to the rolling of the spherical NPs or sliding of the nonspherical NPs between tribopair surfaces [11.161]. For example, the friction and wear of PAO-6 polyalphaolefin lubricant was reduced by 20 and 50%, respectively, when 0.5% ZnO or ZrO_2 was added to the lubricant [11.185]. Abrasive NPs have been used for chemical and mechanical polishing (CMP) of silicon wafers in manufacturing of integrated circuits (IC) [11.161]. For instance, silicon wafers were polished by CeO_2-coated SiO_2 NPs (150−200 nm) with material removal rate of 454 nm/min [11.186].

Ceramic or carbon-based NPs have been added to polymer or metal matrices to make nanocomposites with improved mechanical properties [11.161]. For example, the hardness and tensile strength of an aluminum matrix increased by 115 and 67%, respectively, with the addition of 7 vol.% Al_2O_3 NPs (50 nm) to the matrix [11.187]. The tensile strength and tensile modulus of rubbery epoxy resin increased by fivefold with incorporation of 10 wt% silica NPs [11.188].

In addition of the aforementioned applications, NPs have applications in electronics, textile manufacturing, and water treatment. Semiconducting polymer NPs have been used in organic photovoltaics, field-effect transistors and light-emitting diodes [11.189]. Carbon-coated Sn NPs and Si NPs distributed on graphene sheets were used as anodes while $LiCoPO_4$ NPs were used as cathodes in lithium ion batteries [11.190–192]. Ag NPs due to their antimicrobial properties have been used to produce antimicrobial paints and coatings [11.193, 194]. ZnO and TiO_2 NPs due to their photocatalytic activity have applications in removal of chemical and biological contaminants from water [11.195].

11.5 Summary

NPs can be synthesized from several classes of materials including inorganic (e.g., metal oxide NPs), organic (e.g., polymeric NPs), hybrid and biological materials. Physical techniques (ball milling, vapor deposition and electrospraying) as well as chemical methods (reduction of metal salts, sol-gel, coprecipitation and thermal decomposition) are used for the synthesis of inorganic NPs. Organic NPs can be synthesized via microemulsion, nanoprecipitation, dialysis and rapid expansion of a supercritical solution. Hybrid NPs are composed of both organic and inorganic materials. The inorganic component can form the core or the shell of the hybrid NPs. In addition to the naturally occurring biological NPs, NPs can be synthesized from biomolecules including proteins, peptides and polysaccharides. The physico-mechanical properties of NPs are significantly different from those of bulk materials. For example, the catalytic activity, superparamagnetism, hardness and Coulomb energy of the NPs are higher than those of bulk materials. Due to their unique properties, NPs have applications in a wide range of areas including biosensing, drug delivery, bioimaging, catalysis, nanomanufacturing, lubrication, electronics, textile manufacturing, and water treatment.

Acknowledgments. This work was supported by research grants to E. Jabbari from the United States National Science Foundation under Award Numbers CBET1403545 and IIP150024 and the National Institute of Arthritis and Musculoskeletal and Skin Diseases of the National Institutes of Health under Award Number AR063745. The content is solely the responsibility of the authors and does not necessarily represent the official views of the National Institutes of Health.

References

11.1 C. Dhand, N. Dwivedi, X.J. Loh, A.N.J. Ying, N.K. Verma, R.W. Beuerman, R. Lakshminarayanan, S. Ramakrishna: Methods and strategies for the synthesis of diverse nanoparticles and their applications: A comprehensive overview, RSC Advances **5**, 105003–105037 (2015) doi:10.1039/c5ra19388e

11.2 M. Dossi, R. Ferrari, L. Dragoni, C. Martignoni, P. Gaetani, M. D'Incalci, M. Morbidelli, D. Moscatelli: Synthesis of fluorescent pmma-based nanoparticles, Macromol. Mater. Eng. **298**, 771–778 (2013) doi:10.1002/mame.201200122

11.3 S.L. Pal, U. Jana, P.K. Manna, G.P. Mohanta, R. Manavalan: Nanoparticle: An overview of preparation and characterization, J. Appl. Pharm. Sci. **1**, 228–234 (2011) doi:10.7897/2230-8407.04408

11.4 J.E. Munoz, J. Cervantes, R. Esparza, G. Rosas: Iron nanoparticles produced by high-energy ball milling, J. Nanopar. Res. **9**, 945–950 (2007) doi:10.1007/s11051-007-9226-6

11.5 J.F. de Carvalho, S.N. de Medeiros, M.A. Morales, A.L. Dantas, A.S. Carrico: Synthesis of magnetite nanoparticles by high energy ball milling, Appl. Surf. Sci. **275**, 84–87 (2013) doi:10.1016/j.apsusc.2013.01.118

11.6 V. Bouchat: N, Moreau, J.F. Colomer, S. Lucas: On some applications of nanoparticles synthesized in the gas phase by magnetron discharges, J. Surf. Eng. Mater. Adv. Technol. **3**, 184–189 (2013) doi:10.4236/jsemat.2013.33025

11.7 P.L. Ong, S. Mahmood, T. Zhang, J.J. Lin, R.V. Ramanujan, P. Lee, R.S. Rawat: Synthesis of FeCo nanoparticles by pulsed laser deposition in a diffusion cloud chamber, Appl. Surf. Sci. **254**, 1909–1914 (2008) doi:10.1016/j.apsusc.2007.07.186

11.8 Y.T. Jing, H.W. Wang, X. Chen, X.F. Wang, H.G. Wei, Z.H. Guo: Pulsed laser deposited Ag nanoparticles on nickel hydroxide nanosheet arrays for highly sensitive surface-enhanced Raman scattering spectroscopy, Appl. Surf. Sci. **316**, 66–71 (2014) doi:10.1016/j.apsusc.2014.07.169

11.9 A. Jaworek, A.T. Sobczyk: Electrospraying route to nanotechnology: An overview, J. Electrost. **66**, 197–219 (2008) doi:10.1016/j.elstat.2007.10.001

11.10 M. Valvo, U. Lafont, D. Munao, E.M. Kelder: Electrospraying-assisted synthesis of tin nanoparticles for Li-ion battery electrodes, J. Power Sources **189**, 297–302 (2009) doi:10.1016/j.jpowsour.2008.09.019

11.11 K. Soliwoda, M. Rosowski, E. Tomaszewska, B. Tkacz-Szczesna, G. Celichowski, M. Psarski, J. Grobelny: Synthesis of monodisperse gold nanoparticles via electrospray-assisted chemical reduction method in cyclohexane, Colloids Surf. A **482**, 148–153 (2015) doi:10.1016/j.colsurfa.2015.04.040

11.12 R.G. Chaudhuri, S. Paria: Core/shell nanoparticles: Classes, properties, synthesis mechanisms, characterization, and applications, Chem. Rev. **112**, 2373–2433 (2012) doi:10.1021/cr100449n

11.13 X.Q. Li, W.X. Zhang: Iron nanoparticles: The core-shell structure and unique properties for Ni(II) sequestration, Langmuir **22**, 4638–4642 (2006) doi:10.1021/la060057k

11.14 J.P. Jolivet, C. Froidefond, A. Pottier, C. Chaneac, S. Cassaignon, E. Tronc, P. Euzen: Size tailoring of oxide nanoparticles by precipitation in aqueous medium. A semi-quantitative modelling, J. Mater. Chem. **14**, 3281–3288 (2004) doi:10.1039/b407086k

11.15 A.R. Tao, S. Habas, P.D. Yang: Shape control of colloidal metal nanocrystals, Small **4**, 310–325 (2008) doi:10.1002/smll.200701295

11.16 I.A. Rahman, V. Padavettan: Synthesis of silica nanoparticles by sol-gel: Size-dependent properties, surface modification, and applications in silica-polymer nanocomposites – A review, J. Nanomater. **24**, 015105 (2012) doi:10.1088/0957-4484/24/1/015105

11.17 J. Gautier, E. Allard-Vannier, K. Herve-Aubert, M. Souce, I. Chourpa: Design strategies of hybrid metallic nanoparticles for theragnostic applications, Nanotechnology **24**(43), 432002 (2013) doi:10.1088/0957-4484/24/43/432002

11.18 M. Salavati-Niasari, M. Dadkhah, F. Davar: Synthesis and characterization of pure cubic zirconium oxide nanocrystals by decomposition of bis-aqua, tris-acetylacetonato zirconium(IV) nitrate as new precursor complex, Inorganica Chimica Acta **362**, 3969–3974 (2009) doi:10.1016/j.ica.2009.05.036

11.19 S.Y. Lee, M.T. Harris: Surface modification of magnetic nanoparticles capped by oleic acids: Characterization and colloidal stability in polar solvents, J. Colloid and Interface Sci. **293**, 401–408 (2006) doi:10.1016/j.jcis.2005.06.062

11.20 N. Pinna, G. Garnweitner, M. Antonietti, M. Niederberger: A general nonaqueous route to binary metal oxide nanocrystals involving a C–C bond cleavage, J. Am. Chem. Soc. **127**, 5608–5612 (2005) doi:10.1021/ja042323r

11.21 D.L. Huber, E.L. Venturini, J.E. Martin, P.P. Provencio, R.J. Patel: Synthesis of highly magnetic iron nanoparticles suitable for field structuring using a beta-diketone surfactant, J. Magnetism Magnet. Mater. **278**, 311–316 (2004) doi:10.1016/j.jmmm.2003.12.1317

11.22 R. Kumar, S. Lal: Synthesis of organic nanoparticles and their applications in drug delivery and food nanotechnology: A review, J. Nanomater. Mol. Nanotechnol. **3**, 4 (2014) doi:10.4172/2324-8777.1000150

11.23 I. Sole, A. Maestro, C. Gonzalez, C. Solans, J.M. Gutierrez: Optimization of nano-emulsion preparation by low-energy methods in an ionic surfactant system, Langmuir **22**, 8326–8332 (2006) doi:10.1021/la0613676

11.24 J. Allouche: Synthesis of organic and bioorganic nanoparticles: An overview of the preparation methods. In: *Nanomaterials: A Danger or a Promise?*, ed. by R. Brayner, F. Fiévet, T. Coradin (Springer, London 2013)

11.25 J.C. Lopez-Montilla, P.E. Herrera-Morales, S. Pandey, D.O. Shah: Spontaneous emulsification: Mechanisms, physicochemical aspects, modeling, and applications, J. Dispers. Sci. Technol. **23**, 219–268 (2002) doi:10.1080/01932690208984202

11.26 P. Fernandez, V. Andre, J. Rieger, A. Kuhnle: Nano-emulsion formation by emulsion phase inversion, Colloids Surf. A **251**, 53–58 (2004) doi:10.1016/

j.colsurfa.2004.09.029
11.27 R.L. McCall, R.W. Sirianni: PLGA nanoparticles formed by single- or double-emulsion with vitamin E-TPGS, Jove-J. Visualized Exp. **27**(82), 51015 (2013) doi:10.3791/51015
11.28 J. Singh, S. Pandit, V.W. Bramwell, H.O. Alpar: Diphtheria toxoid loaded poly-(epsilon-caprolactone) nanoparticles as mucosal vaccine delivery systems, Methods **38**, 96–105 (2006) doi:10.1016/j.ymeth.2005.11.003
11.29 C.X. Song, V. Labhasetwar, H. Murphy, X. Qu, W.R. Humphrey, R.J. Shebuski, R.J. Levy: Formulation and characterization of biodegradable nanoparticles for intravascular local drug delivery, J. Control. Release **43**, 197–212 (1997) doi:10.1016/S0168-3659(96)01484-8
11.30 J. Allouche, M. Boissiere, C. Helary, J. Livage, T. Coradin: Biomimetic core-shell gelatine/silica nanoparticles: A new example of biopolymer-based nanocomposites, J. Mater. Chem. **16**, 3120–3125 (2006) doi:10.1039/b604366f
11.31 C. Damge, C.P. Reis, N. Ubrich, P. Maincent, F. Veiga, A. Ribeiro: Alginate-based insulin nanoparticles – Dextrane for oral administration in the diabetic rat, Diabetes Metab. **33**, S67–S67 (2007) doi:10.1186/s12951-015-0136-y
11.32 D. Barati, S.R.P. Shariati, S. Moeinzadeh, J.M. Melero-Martin, A. Khademhosseini, E. Jabbari: Spatiotemporal release of BMP-2 and VEGF enhances osteogenic and vasculogenic differentiation of human mesenchymal stem cells and endothelial colony-forming cells co-encapsulated in a patterned hydrogel, J. Control. Release **223**, 126–136 (2016) doi:10.1016/j.jconrel.2015.12.031
11.33 J.N.L. De Avila, L.L.G.C. De Araujo, S. Drexler, J.D. Rodrigues, R.S.V. Nascimento: Polystyrene nanoparticles as surfactant carriers for enhanced oil recovery, J. Appl. Polymer Sci. **133**, 43789 (2016) doi:10.1002/app.43789
11.34 S.J. Yoon, H. Chun, M.S. Lee, N. Kim: Preparation of poly(N-vinylcarbazole) (PVK) nanoparticles by emulsion polymerization and PVK hollow particles, Synth. Metals **159**, 518–522 (2009) doi:10.1016/j.synthmet.2008.11.011
11.35 A.M. Oliveira, K.L. Guimaraes, N.N.P. Cerize: The role of functional monomers on producing nanostructured lattices obtained by surfactant-free emulsion polymerization – A novel approach, Eur. Polym. J. **71**, 268–278 (2015) doi:10.1016/j.eurpolymj.2015.07.049
11.36 B.V.N. Nagavarma, K.S.Y. Hemant, A. Ayaz, L.S. Vasudha, H.G. Shivakumar: Different techniques for preparation of polymeric nanoparticles – A review, Asian J. Pharm. Clin. Res. **5**(3), 16–23 (2012)
11.37 C.P. Reis, R.J. Neufeld, A.J. Ribeiro, F. Veiga: Nanoencapsulation I. Methods for preparation of drug-loaded polymeric nanoparticles, Nanomedicine **2**, 8–21 (2006) doi:10.1016/j.nano.2005.12.003
11.38 T. Musumeci, C.A. Ventura, C. Carbone, R. Pignatello, G. Puglisi: Effects of external phase on D-cycloserine loaded W/O nanocapsules prepared by the interfacial polymerization method, Eur. J. Med. Chem. **46**, 2828–2834 (2011) doi:10.1016/j.ejmech.2011.04.003
11.39 S. Watnasirichaikul, N.M. Davies, T. Rades, I.G. Tucker: Preparation of biodegradable insulin nanocapsules from biocompatible microemulsions, Pharm. Res. **17**, 684–689 (2000) doi:10.1023/A:1007574030674
11.40 S. Kuypers, S.K. Pramanik, L. D'Olieslaeger, G. Reekmans, M. Peters, J. D'Haen, D. Vanderzande, T. Junkers, P. Adriaensens, A. Ethirajan: Interfacial thiol-isocyanate reactions for functional nanocarriers: A facile route towards tunable morphologies and hydrophilic payload encapsulation, Chem. Commun. **51**, 15858–15861 (2015) doi:10.1039/c5cc05258k
11.41 M.J. Monteiro, M.F. Cunningham: Polymer nanoparticles via living radical polymerization in aqueous dispersions: Design and applications, Macromolecules **45**, 4939–4957 (2012) doi:10.1021/ma300170c
11.42 K.O. Sebakhy, S. Kessel, M.J. Monteiro: Nanoreactors to synthesize well-defined polymer nanoparticles: Decoupling particle size from molecular weight, Macromolecules **43**, 9598–9600 (2010) doi:10.1021/ma1019889
11.43 C. Dire, S. Magnet, L. Couvreur, B. Charleux: Nitroxide-mediated controlled/living free-radical surfactant-free emulsion polymerization of methyl methacrylate using a poly(methacrylic acid)-based macroalkoxyamine initiator, Macromolecules **42**, 95–103 (2009) doi:10.1021/ma802083g
11.44 R. Gonzalez-Blanco, M.F. Cunningham, E. Saldivar-Guerra: High solids TEMPO-mediated radical semibatch emulsion polymerization of styrene, J. Polym. Sci. Part A **54**, 49–62 (2016) doi:10.1002/pola.27771
11.45 J. Nicolas, A.V. Ruzette, C. Farcet, P. Gerard, S. Magnet, B. Charleux: Nanostructured latex particles synthesized by nitroxide-mediated controlled/living free-radical polymerization in emulsion, Polymer **48**, 7029–7040 (2007) doi:10.1016/j.polymer.2007.09.039
11.46 W.W. Li, K. Matyjaszewski, K. Albrecht, M. Moller: Reactive surfactants for polymeric nanocapsules via interfacially confined miniemulsion ATRP, Macromolecules **42**, 8228–8233 (2009) doi:10.1021/ma901574y
11.47 K. Min, H. Gao, J.A. Yoon, W. Wu, T. Kowalewski, K. Matyjaszewski: One-pot synthesis of hairy nanoparticles by emulsion ATRP, Macromolecules **42**, 1597–1603 (2009) doi:10.1021/ma8026244
11.48 D.J. Siegwart, A. Srinivasan, S.A. Bencherif, A. Karunanidhi, J.K. Oh, S. Vaidya, R. Jin, J.O. Hollinger, K. Matyjaszewki: Cellular uptake of functional nanogels prepared by inverse miniemulsion atrp with encapsulated proteins, carbohydrates, and gold nanoparticles, Biomacromolecules **10**, 2300–2309 (2009) doi:10.1021/bm9004904

11.49 F.Y. Cheng, S.P.H. Wang, C.H. Su, T.L. Tsai, P.C. Wu, D.B. Shieh, J.H. Chen, P.C.H. Hsieh, C.S. Yeh: Stabilizer-free poly(lactide-co-glycolide) nanoparticles for multimodal biomedical probes, Biomaterials **29**, 2104–2112 (2008) doi:10.1016/j.biomaterials.2008.01.01

11.50 P. Legrand, S. Lesieur, A. Bochot, R. Gref, W. Raatjes, G. Barratt, C. Vauthier: Influence of polymer behaviour in organic solution on the production of polylactide nanoparticles by nanoprecipitation, Int. J. Pharm. **344**, 33–43 (2007) doi:10.1016/j.ijpbarm.2007.05.054

11.51 S.K. Pandey, C. Haldar, D.K. Vishwas, P. Maiti: Synthesis and in vitro evaluation of melatonin entrapped PLA nanoparticles: An oxidative stress and T-cell response using golden hamster, J. Biomed. Mater. Res. A **103**, 3034–3044 (2015) doi:10.1002/jbm.a.35441

11.52 S.K. Pandey, D.K. Patel, A.K. Maurya, R. Thakur, D.P. Mishra, M. Vinayak, C. Haldar, P. Maiti: Controlled release of drug and better bioavailability using poly(lacticacid-co-glycolic acid) nanoparticles, Int. J. Biol. Macromol. **89**, 99–110 (2016) doi:10.1016/j.ijbiomac.2016.04.065

11.53 K. Sawant, A. Pandey, S. Patel: Aripiprazole loaded poly(caprolactone) nanoparticles: Optimization and in vivo pharmacokinetics, Mater. Sci. Eng. C **66**, 230–243 (2016) doi:10.1016/j.msec.2016.04.089

11.54 Z. Zili, S. Sfar, H. Fessi: Preparation and characterization of poly-e-caprolactone nanoparticles containing griseofulvin, Int. J. Pharm. **294**, 261–267 (2005) doi:10.1016/j.ijpharm.2005.01.020

11.55 A.O. Elzoghby: Gelatin-based nanoparticles as drug and gene delivery systems: Reviewing three decades of research, J. Control. Release **172**, 1075–1091 (2013) doi:10.1016/j.jconrel.2013.09.019

11.56 L. Songtipya, M.C. Thies, A. Sane: Effect of rapid expansion of subcritical solutions processing conditions on loading capacity of tetrahydrocurcumin encapsulated in poly(L-lactide) particles, J. Supercrit. Fluids **113**, 119–127 (2016) doi:10.1016/j.supflu.2016.03.020

11.57 S.K. Sharma, R. Jagannathan: High throughput RESS processing of sub-10 nm ibuprofen nanoparticles, J. Supercrit. Fluids **109**, 74–79 (2016) doi:10.1016/j.supflu.2015.11.019

11.58 M. Turk, D. Bolten: Formation of submicron poorly water-soluble drugs by rapid expansion of supercritical solution (RESS): Results for Naproxen, J. Supercrit. Fluids **55**, 778–785 (2010) doi:10.1016/j.supflu.2010.09.023

11.59 J.P. Chapel, J.F. Berret: Versatile electrostatic assembly of nanoparticles and polyelectrolytes: Coating, clustering and layer-by-layer processes, Curr. Opin. Colloid Interface Sci. **17**, 97–105 (2012) doi:10.1016/j.cocis.2011.08.009

11.60 G. Schneider, G. Decher: Functional core/shell nanoparticles via layer-by-layer assembly. Investigation of the experimental parameters for controlling particle aggregation and for enhancing dispersion stability, Langmuir **24**, 1778–1789 (2008) doi:10.1021/la7021837

11.61 A. Aqil, S. Vasseur, E. Duguet, C. Passirani, J.P. Benoit, A. Roch, R. Muller, R. Jerome, C. Jerome: PEO coated magnetic nanoparticles for biomedical application, Eur. Polym. J. **44**, 3191–3199 (2008) doi:10.1016/j.eurpolymj.2008.07.011

11.62 P. Froimowicz, R. Munoz-Espi, K. Landfester, A. Musyanovych, D. Crespy: Surface-functionalized particles: From their design and synthesis to materials science and bio-applications, Curr. Org. Chem. **17**, 900–912 (2013) doi:10.2174/1385272811317090004

11.63 E.J. Tang, G.X. Cheng, X.L. Ma, X.S. Pang, Q. Zhao: Surface modification of zinc oxide nanoparticle by PMAA and its dispersion in aqueous system, Appl. Surf. Sci. **252**, 5227–5232 (2006) doi:10.1016/j.apsusc.2005.08.004

11.64 M.N. Tchoul, S.P. Fillery, H. Koerner, L.F. Drummy, F.T. Oyerokun, P.A. Mirau, M.F. Durstock, R.A. Vaia: Assemblies of titanium dioxide-polystyrene hybrid nanoparticles for dielectric applications, Chem. Mater. **22**, 1749–1759 (2010), doi:10.1021/cm903182n

11.65 M. Li, L.Q. Xu, L. Wang, Y.P. Wu, J. Li, K.G. Neoh, E.T. Kang: Clickable poly(ester amine) dendrimer-grafted Fe304 nanoparticles prepared via successive Michael addition and alkyne-azide click chemistry, Polym. Chem. **2**, 1312–1321 (2011) doi:10.1039/c1py00084e

11.66 S. Kango, S. Kalia, A. Celli, J. Njuguna, Y. Habibi, R. Kumar: Surface modification of inorganic nanoparticles for development of organic-inorganic nanocomposites-A review, Prog. Polym. Sci. **38**, 1232–1261 (2013) doi:10.1016/j.progpolymsci.2013.02.003

11.67 T. von Werne, T.E. Patten: Atom transfer radical polymerization from nanoparticles: A tool for the preparation of well-defined hybrid nanostructures and for understanding the chemistry of controlled/living radical polymerizations from surfaces, J. Am. Chem. Soc. **123**, 7497–7505 (2001) doi:10.1021/Ja010235q

11.68 A. Khabibullin, K. Bhangaonkar, C. Mahoney, Z. Lu, M. Schmitt, A.K. Sekizkardes, M.R. Bockstaller, K. Matyjaszewski: Grafting PMMA brushes from alpha-alumina nanoparticles via SI-ATRP, ACS Appl. Mater. Interfaces **8**, 5458–5465 (2016) doi:10.1021/acsami.5b12311

11.69 H.D. Wang, W.Q. Luo, J.C. Chen: Fabrication and characterization of thermoresponsive Fe304@PNIPAM hybrid nanomaterials by surface-initiated RAFT polymerization, J. Mater. Sci. **47**, 5918–5925 (2012) doi:10.1007/s10853-012-6493-0

11.70 M.A. Hood, M. Mari, R. Munoz-Espi: Nanodroplet, Materials **7**, 4057–4087 (2014) doi:10.3390/ma7054057

11.71 E. Bourgeat-Lami, G.A. Farzi, L. David, J.L. Putaux, T.F.L. McKenna: Silica encapsulation by miniemulsion polymerization: distribution and localization of the silica particles in droplets and latex particles, Langmuir **28**, 6021–6031 (2012) doi:10.1021/la300587b

11.72 Z.X. Chen, Y.H. Zhang, L.L. Duan, Z.G. Wang, Y.L. Li, P.X. He: Preparation of PSt/SiO_2 nanoparticles with raspberry-like structure via nonionic surfactant miniemulsion polymerization, J. Adhes. Sci. Technol. **29**, 2117–2129 (2015) doi:10.1080/01694243.2015.1057396

11.73 M.M. Rahim-Abadi, A.R. Mandavian, A. Gharieh, H. Salehi-Mobarakeh: Chemical modification of Ti02 nanoparticles as an effective way for encapsulation in polyacrylic shell via emulsion polymerization, Prog. Org. Coat. **88**, 310–315 (2015) doi:10.1016/j.porgcoat.2015.07.013

11.74 A. Perro, S. Reculusa, E. Bourgeat-Lami, E. Duguet, S. Ravaine: Synthesis of hybrid colloidal particles: From snowman-like to raspberry-like morphologies, Colloids Surf. A **284**, 78–83 (2006) doi:10.1016/j.colsurfa.2005.11.073

11.75 C.S. Wagner, S. Shehata, K. Henzler, J.Y. Yuan, A. Wittemann: Towards nanoscale composite particles of dual complexity, J. Colloid Interface Sci. **355**, 115–123 (2011) doi:10.1016/j.jcis.2010.12.017

11.76 Q.J. Luo, R.J. Hickey, S.J. Park: Controlling the location of nanoparticles in colloidal assemblies of amphiphilic polymers by tuning nanoparticle surface chemistry, ACS Macro Lett. **2**, 107–111 (2013) doi:10.1021/mz3006044

11.77 M. Agrawal, J. Rubio-Retama, N.E. Zafeiropoulos, N. Gaponik, S. Gupta, V. Cimrova, V. Lesnyak, E. Lopez-Cabarcos, S. Tzavalas, R. Rojas-Reyna, A. Eychmuller, M. Stamm: Switchable photoluminescence of CdTe nanocrystals by temperature-responsive microgels, Langmuir **24**, 9820–9824 (2008) doi:10.1021/la801347d

11.78 M. Schrinner, M. Ballauff, Y. Talmon, Y. Kauffmann, J. Thun, M. Moller, J. Breu: Single nanocrystals of platinum prepared by partial dissolution of Au-Pt nanoalloys, Science **323**, 617–620 (2009) doi:10.1126/science.1166703

11.79 V. Fischer, I. Lieberwirth, G. Jakob, K. Landfester, R. Munoz-Espi: Metal oxide/polymer hybrid nanoparticles with versatile functionality prepared by controlled surface crystallization, Adv. Funct. Mater. **23**, 451–466 (2013) doi:10.1002/adfm.201201839

11.80 A. Ethirajan, U. Ziener, K. Landfester: Surface-functionalized polymeric nanoparticles as templates for biomimetic mineralization of hydroxyapatite, Chem. Mater. **21**, 2218–2225 (2009) doi:10.1021/cm9001724

11.81 D. Barati, J.D. Walters, S.R.P. Shariati, S. Moeinzadeh, E. Jabbari: Effect of organic acids on calcium phosphate nucleation and osteogenic differentiation of human mesenchymal stem cells on peptide functionalized nanofibers, Langmuir **31**, 5130–5140 (2015) doi:10.1021/acs.langmuir.5b00615

11.82 O. Karaman, A. Kumar, S. Moeinzadeh, X.Z. He, T. Cui, E. Jabbari: Effect of surface modification of nanofibres with glutamic acid peptide on calcium phosphate nucleation and osteogenic differentiation of marrow stromal cells, J. Tissue Eng. Regen. Med. **10**, E132–E146 (2016) doi:10.1002/term.1775

11.83 A. Schrade, K. Landfester, U. Ziener: Pickering-type stabilized nanoparticles by heterophase polymerization, Chem. Soc. Rev. **42**, 6823–6839 (2013) doi:10.1039/c3cs60100e

11.84 M.J. Percy, C. Barthet, J.C. Lobb, M.A. Khan, S.F. Lascelles, M. Vamvakaki, S.P. Armes: Synthesis and characterization of vinyl polymer-silica colloidal nanocomposites, Langmuir **16**, 6913 (2000) doi:10.1021/la0004294

11.85 A. Schmid, S.P. Armes, C.A.P. Leite, F. Galembeck: Efficient preparation of polystyrene/silica colloidal nanocomposite particles by emulsion polymerization using a glycerol-functionalized silica sol, Langmuir **25**, 2486–2494 (2009)

11.86 J.H. Chen, C.Y. Cheng, W.Y. Chiu, C.F. Lee, N.Y. Liang: Synthesis of ZnO/polystyrene composites particles by Pickering emulsion polymerization, Eur. Polym. J. **44**, 3271–3279 (2008) doi:10.1016/j.eurpolymj.2008.07.023

11.87 S. Stanley: Biological nanoparticles and their influence on organisms, Curr. Opin. Biotechnol. **28**, 69–74 (2014) doi:10.1016/j.copbio.2013.11.014

11.88 C.S. Thaxton, J.S. Rink, P.C. Naha, D.P. Cormode: Lipoproteins and lipoprotein mimetics for imaging and drug delivery, Adv. Drug Deliv. Rev. **106**, 116–131 (2016)

11.89 N. Sabnis, M. Nair, M. Israel, W.J. McConathy, A.G. Lacko: Enhanced solubility and functionality of valrubicin (AD-32) against cancer cells upon encapsulation into biocompatible nanoparticles, Int. J. Nanomed. **7**, 975–983 (2012) doi:10.2147/ijn.S28029

11.90 K.B. Johnsen, J.M. Gudbergsson, M.N. Skov, L. Pilgaard, T. Moos, M. Duroux: A comprehensive overview of exosomes as drug delivery vehicles – Endogenous nanocarriers for targeted cancer therapy, Biochim. Biophys. Acta **1846**, 75–87 (2014) doi:10.1016/j.bbcan.2014.04.005

11.91 B.S. Batista, W.S. Eng, K.T. Pilobello, K.D. Hendricks-Munoz, L.K. Mahal: Identification of a conserved glycan signature for microvesicles, J. Proteome Res. **10**, 4624–4633 (2011) doi:10.1021/pr200434y

11.92 F.T. Borges, S.A. Melo, B.C. Ozdemir, N. Kato, I. Revuelta, C.A. Miller, V.H. Gattone, V.S. LeBleu, R. Kalluri: TGF-beta 1-containing exosomes from injured epithelial cells activate fibroblasts to initiate tissue regenerative responses and fibrosis, J. Am. Soc. Nephrol. **24**, 385–392 (2013) doi:10.1681/Asn.2012101031

11.93 G. Raposo, H.W. Nijman, W. Stoorvogel, R. Leijendekker, C.V. Harding, C.J.M. Melief, H.J. Geuze: B lymphocytes secrete antigen-presenting vesicles, J. Exp. Med. **183**, 1161–1172 (1996) doi:10.1084/jem.183.3.1161

11.94 T.N. Lamichhane, S. Sokic, J.S. Schardt, R.S. Raiker, J.W. Lin, S.M. Jay: Emerging roles for extracellular vesicles in tissue engineering and regenerative medicine, Tissue Eng. Part B Rev. **21**, 45–54 (2015) doi:10.1089/ten.teb.2014.0300

11.95 M. Allen, D. Willits, J. Mosolf, M. Young, T. Douglas: Protein cage constrained synthesis of ferrimagnetic iron oxide nanoparticles, Adv. Mater. **14**, 1562 (2002) doi:10.1002/1521-4095(20021104)14:21<1562::Aid-Adma1562>3.0.Co;2-D

11.96 I. Yamashita, K. Iwahori, S. Kumagai: Ferritin in the field of nanodevices, Biochim. Biophys. Acta-Gen. Subjects **1800**, 846–857 (2010) doi:10.1016/j.bbagen.2010.03.005

11.97 K.L. Fan, C.Q. Cao, Y.X. Pan, D. Lu, D.L. Yang, J. Feng, L.N. Song, M.M. Liang, X.Y. Yan: Magnetoferritin nanoparticles for targeting and visualizing tumour tissues, Nat. Nanotechnol. **7**, 459–464 (2012) doi:10.1038/Nnano.2012.90

11.98 D. Yan, Y.Q. Wei, H.C. Guo, S.Q. Sun: The application of virus-like particles as vaccines and biological vehicles, Appl. Microbiol. Biotechnol. **99**, 10415–10432 (2015) doi:10.1007/s00253-015-7000-8

11.99 Z.J. Wu, K.V. Chen, I. Yildiz, A. Dirksen, R. Fischer, P.E. Dawson, N.F. Steinmetz: Development of viral nanoparticles for efficient intracellular delivery, Nanoscale **4**, 3567–3576 (2012) doi:10.1039/c2nr30366c

11.100 D.P. Patterson, A. Rynda-Apple, A.L. Harmsen, A.G. Harmsen, T. Douglas: Biomimetic antigenic nanoparticles elicit controlled protective immune response to influenza, ACS Nano **7**, 3036–3044 (2013) doi:10.1021/nn4006544

11.101 W. Lohcharoenkal, L.Y. Wang, Y.C. Chen, Y. Rojanasakul: Protein nanoparticles as drug delivery carriers for cancer therapy, Biomed Res. Int. **2014**, 180549 (2014)

11.102 L.P.H. Estrada, J.A. Champion: Protein nanoparticles for therapeutic protein delivery, Biomater. Sci. **3**, 787–799 (2015) doi:10.1039/c5bm00052a

11.103 K. Langer, M.G. Anhorn, I. Steinhauser, S. Dreis, D. Celebi, I. Schrickel, S. Faust, V. Vogel: Human serum albumin (HSA) nanoparticles: Reproducibility of preparation process and kinetics of enzymatic degradation, Int. J. Pharm. **347**, 109–117 (2008) doi:10.1016/j.ijpharm.2007.06.028

11.104 G.L. Wang, K. Siggers, S.F. Zhang, H.X. Jiang, Z.H. Xu, R.F. Zernicke, J. Matyas, H. Uludag: Preparation of BMP-2 containing bovine serum albumin (BSA) nanoparticles stabilized by polymer coating, Pharm. Res. **25**, 2896–2909 (2008) doi:10.1007/s11095-008-9692-2

11.105 G. Kaul, M. Amiji: Biodistribution and targeting potential of poly(ethylene glycol)-modified gelatin nanoparticles in subcutaneous murine tumor model, J. Drug Target. **12**, 585–591 (2004) doi:10.1080/10611860400013451

11.106 A.O. Elzoghby, M.W. Helmy, W.M. Samy, N.A. Elgindy: Novel ionically crosslinked casein nanoparticles for flutamide delivery: formulation, characterization, and in vivo pharmacokinetics, Int. J. Nanomed. **8**, 1721–1732 (2013) doi:10.2147/Ijn.S40674

11.107 L. Yang, F. Cui, D.M. Cun, A. Tao, K. Shi, W.H. Lin: Preparation, characterization and biodistribution of the lactone form of 10-hydroxycamptothecin (HCPT)-loaded bovine serum albumin (BSA) nanoparticles, Int. J. Pharm. **340**, 163–172 (2007) doi:10.1016/j.ijpharm.2007.03.028

11.108 S. Rhaese, H. von Briesen, H. Rubsamen-Waigmann, J. Kreuter, K. Langer: Human serum albumin-polyethylenimine nanoparticles for gene delivery, J. Control. Release **92**, 199–208 (2003) doi:10.1016/S0168-3659(03)00302-X

11.109 I.W. Hamley: Self-assembly of amphiphilic peptides, Soft Matter **7**, 4122–4138 (2011) doi:10.1039/c0sm01218a

11.110 S.K. Nitta, K. Numata: Biopolymer-based nanoparticles for drug/gene delivery and tissue engineering, Int. J. Mol. Sci. **14**, 1629–1654 (2013) doi:10.3390/ijms14011629

11.111 S. Santoso, W. Hwang, H. Hartman, S.G. Zhang: Self-assembly of surfactant-like peptides with variable glycine tails to form nanotubes and nanovesicles, Nano Lett. **2**, 687–691 (2002) doi:10.1021/nl025563i

11.112 G. von Maltzahn, S. Vauthey, S. Santoso, S.U. Zhang: Positively charged surfactant-like peptides self-assemble into nanostructures, Langmuir **19**, 4332–4337 (2003) doi:10.1021/la026526+

11.113 E. Jabbari, X.M. Yang, S. Moeinzadeh, X.Z. He: Drug release kinetics, cell uptake, and tumor toxicity of hybrid VVVVVKK peptide-assembled polylactide nanoparticles, Eur. J. Pharm. Biopharm. **84**, 49–62 (2013) doi:10.1016/j.ejpb.2012.12.012

11.114 H.G. Cui, M.J. Webber, S.I. Stupp: Self-assembly of peptide amphiphiles: From molecules to nanostructures to biomaterials, Biopolymers **94**, 1–18 (2010) doi:10.1002/bip.21328

11.115 A. Dehsorkhi, V. Castelletto, I.W. Hamley: Self-assembling amphiphilic peptides, J. Pept. Sci. **20**, 453–467 (2014) doi:10.1002/psc.2633

11.116 I.W. Hamley, A. Dehsorkhi, V. Castelletto, S. Furzeland, D. Atkins, J. Seitsonen, J. Ruokolainen: Reversible helical unwinding transition of a self-assembling peptide amphiphile, Soft Matter **9**, 9290–9293 (2013) doi:10.1039/c3sm51725j

11.117 S. Eskandari, T. Guerin, I. Toth, R.J. Stephenson: Recent advances in self-assembled peptides: Implications for targeted drug delivery and vaccine engineering, Adv. Drug Deliv. Rev. (2016) doi:10.1016/j.addr.2016.06.013, in press

11.118 R. Herrero-Vanrell, A.C. Rincon, M. Alonso, V. Reboto, I.T. Molina-Martinez, J.C. Rodriguez-Cabello: Self-assembled particles of an elastin-like polymer as vehicles for controlled drug release, J. Control. Release **102**, 113–122 (2005) doi:10.1016/j.jconrel.2004.10.001

11.119 A. Yeboah, R.I. Cohen, R. Faulknor, R. Schloss, M.L. Yarmush, F. Berthiaume: The development and characterization of SDF1 alpha-elastin-like-peptide nanoparticles for wound healing, J. Control. Release **232**, 238–247 (2016) doi:10.1016/j.jconrel.2016.04.020

11.120 J. Rodriguez-Hernandez, S. Lecommandoux: Reversible inside-out micellization of pH-responsive and water-soluble vesicles based on polypeptide diblock copolymers, J. Am. Chem.

Soc. **127**, 2026–2027 (2005) doi:10.1021/ja043920g
11.121 B. Sarmento, A.J. Ribeiro, F. Veiga, D.C. Ferreira, R.J. Neufeld: Insulin-loaded nanoparticles are prepared by alginate ionotropic pre-gelation followed by chitosan polyelectrolyte complexation, J. Nanosci. Nanotechnol. **7**, 2833–2841 (2007) doi:10.1166/jnn.2007.609
11.122 R.Y. Rasente, J.C. Imperiale, J.M. Lazaro-Martinez, L. Gualco, R. Oberkersch, A. Sosnik, G.C. Calabrese: Dermatan sulfate/chitosan polyelectrolyte complex with potential application in the treatment and diagnosis of vascular disease, Carbohydr. Polym. **144**, 362–370 (2016) doi:10.1016/j.carbpol.2016.02.046
11.123 K.A. Janes, P. Calvo, M.J. Alonso: Polysaccharide colloidal particles as delivery systems for macromolecules, Adv. Drug Deliv. Rev. **47**, 83–97 (2001) doi:10.1016/S0169-409x(00)00123-X
11.124 Y. Cho, J.T. Kim, H.J. Park: Preparation, characterization, and protein loading properties of N-acyl chitosan nanoparticles, J. Appl. Polym. Sci. **124**, 1366–1371 (2012) doi:10.1002/app.34931
11.125 G. Shi, Y.X. Che, Y.M. Zhou, X. Bai, C.H. Ni: Synthesis of polyglycolic acid grafting from sodium alginate through direct polycondensation and its application as drug carrier, J. Mater. Sci. **50**, 7835–7841 (2015) doi:10.1007/s10853-015-9363-8
11.126 C.J. Brinker, G.W. Scherer: *Sol-Gel Science: The Physics and Chemistry of Sol-Gel Processing* (Academic, San Diego 1990)
11.127 A.G. Kolhatkar, A.C. Jamison, D. Litvinov, R.C. Willson, T.R. Lee: Tuning the magnetic properties of nanoparticles, Int. J. Mol. Sci. **14**, 15977–16009 (2013) doi:10.3390/ijms140815977
11.128 C. Burda, X.B. Chen, R. Narayanan, M.A. El-Sayed: Chemistry and properties of nanocrystals of different shapes, Chem. Rev. **105**, 1025–1102 (2005) doi:10.1021/cr030063a
11.129 F. Alexis, E. Pridgen, L.K. Molnar, O.C. Farokhzad: Factors affecting the clearance and biodistribution of polymeric nanoparticles, Mol. Pharm. **5**, 505–515 (2008) doi:10.1021/mp800051m
11.130 J.P. Jolivet, S. Cassaignon, C. Chaneac, D. Chiche, O. Durupthy, D. Portehault: Design of metal oxide nanoparticles: Control of size, shape, crystalline structure and functionalization by aqueous chemistry, C.R. Chimie **13**, 40–51 (2010) doi:10.1016/j.crci.2009.09.012
11.131 A.M. Perez-Coronado, L. Calvo, N. Alonso-Morales, F. Heras, J.J. Rodriguez, M.A. Gilarranz: Multiple approaches to control and assess the size of Pd nanoparticles synthesized via water-in-oil microemulsion, Colloids Surf. A **497**, 28–34 (2016) doi:10.1016/j.colsurfa.2016.02.012
11.132 D. Lemoine, V. Preat: Polymeric nanoparticles as delivery system for influenza virus glycoproteins, J. Control. Release **54**, 15–27 (1998) doi:10.1016/S0168-3659(97)00241-1
11.133 I. Lisiecki, M.P. Pileni: Copper metallic particles synthesized in-situ in reverse micelles - influence of various parameters on the size of the particles, J. Phys. Chem. **99**, 5077–5082 (1995) doi:10.1021/J100014a030
11.134 M. Husein, E. Rodil, J.H. Vera: Formation of silver bromide precipitate of nanoparticles in a single microemulsion utilizing the surfactant counterion, J. Colloid Interface Sci. **273**, 426–434 (2004) doi:10.1016/j.jcis.2004.02.057
11.135 N.M. Husein, E. Rodil, J.H. Vera: Preparation of AgBr nanoparticles in microemulsions via reaction of AgNO3 with CTAB counterion, J. Nanoparticle Res. **9**, 787–796 (2007) doi:10.1007/s11051-006-9107-4
11.136 S. Schubert, J.T. Delaney, U.S. Schubert: Nanoprecipitation and nanoformulation of polymers: from history to powerful possibilities beyond poly(lactic acid), Soft Matter **7**, 1581–1588 (2011) doi:10.1039/c0sm00862a
11.137 H.J. Jeon, J.I. Jeong, M.K. Jang, Y.H. Park, J.W. Nah: Effect of solvent on the preparation of surfactant-free poly(DL-lactide-co-glycolide) nanoparticles and norfloxacin release characteristics, Int. J. Pharm. **207**, 99–108 (2000) doi:10.1016/S0378-5173(00)00537-8
11.138 A.E. Mercado, J. Ma, X. He, E. Jabbari: Release characteristics and osteogenic activity of recombinant human bone morphogenetic protein-2 grafted to novel self-assembled poly(lactide-co-glycolide fumarate) nanoparticles, J. Control. Release **140**, 148–156 (2009) doi:10.1016/j.jconrel.2009.08.009
11.139 H. Mistry, F. Behafarid, E. Zhou, L.K. Ono, L. Zhang, B.R. Cuenya: Shape-dependent catalytic oxidation of 2-butanol over Pt nanoparticles supported on gamma-Al203, ACS Catalysis **4**, 109–115 (2014) doi:10.1021/cs400888n
11.140 N.P. Truong, M.R. Whittaker, C.W. Mak, T.P. Davis: The importance of nanoparticle shape in cancer drug delivery, Expert Opin. Drug Deliv. **12**, 129–142 (2015) doi:10.1517/17425247.2014.950564
11.141 A. Tao, P. Sinsermsuksakul, P.D. Yang: Polyhedral silver nanocrystals with distinct scattering signatures, Angew. Chem. Int. Ed. **45**, 4597–4601 (2006) doi:10.1002/anie.200601277
11.142 L.A. Renna, C.J. Boyle, T.S. Gehan, D. Venkataraman: Polymer nanoparticle assemblies: A versatile route to functional mesostructures, Macromolecules **48**, 6353–6368 (2015) doi:10.1021/acs.macromol.5b00375
11.143 J.A. Champion, Y.K. Katare, S. Mitragotri: Particle shape: A new design parameter for micro- and nanoscale drug delivery carriers, J. Control. Release **121**, 3–9 (2007) doi:10.1016/j.jconrel.2007.03.022
11.144 Y.P. Wang, T.J. Merkel, K. Chen, C.A. Fromen, D.E. Betts, J.M. DeSimone: Generation of a library of particles having controlled sizes and shapes via the mechanical elongation of master templates, Langmuir **27**, 524–528 (2011) doi:10.1021/la1045095
11.145 P. Dalhaimer, A.J. Engler, R. Parthasarathy, D.E. Discher: Targeted worm micelles, Biomacromolecules **5**, 1714–1719 (2004) doi:10.1021/bm049884v

11.146 A.H. Lu, E.L. Salabas, F. Schuth: Magnetic nanoparticles: Synthesis, protection, functionalization, and application, Angew. Chem. Int. Ed. **46**, 1222–1244 (2007) doi:10.1002/anie.200602866

11.147 M. Arruebo, R. Fernandez-Pacheco, M.R. Ibarra, J. Santamaria: Magnetic nanoparticles for drug delivery, Nano Today **2**, 22–32 (2007) doi:10.1016/S1748-0132(07)70084-1

11.148 M. Knobel, W.C. Nunes, L.M. Socolovsky, E. De Biasi, J.M. Vargas, J.C. Denardin: Superparamagnetism and other magnetic features in granular materials: A review on ideal and real systems, J. Nanosci. Nanotechnol. **8**, 2836–2857 (2008) doi:10.1166/Jnn.2008.017

11.149 A. Demortiere, P. Panissod, B.P. Pichon, G. Pourroy, D. Guillon, B. Donnio, S. Begin-Colin: Size-dependent properties of magnetic iron oxide nanocrystals, Nanoscale **3**, 225–232 (2011) doi:10.1039/c0nr00521e

11.150 G.L. Zhen, B.W. Muir, B.A. Moffat, P. Harbour, K.S. Murray, B. Moubaraki, K. Suzuki, I. Madsen, N. Agron-Olshina, L. Waddington, P. Mulvaney, P.G. Hartley: Comparative study of the magnetic behavior of spherical and cubic superparamagnetic iron oxide nanoparticles, J. Phys. Chem. C **115**, 327–334 (2011) doi:10.1021/jp104953z

11.151 K.M. Krishnan: Biomedical nanomagnetics: A spin through possibilities in imaging, diagnostics, and therapy, IEEE Trans. Magn. **46**, 2523–2558 (2010) doi:10.1109/Tmag.2010.2046907

11.152 J.H. Lee, Y.M. Huh, Y. Jun, J. Seo, J. Jang, H.T. Song, S. Kim, E.J. Cho, H.G. Yoon, J.S. Suh, J. Cheon: Artificially engineered magnetic nanoparticles for ultra-sensitive molecular imaging, Nat. Med. **13**, 95–99 (2007) doi:10.1038/nm1467

11.153 N. Shamim, L. Hong, K. Hidajat, M.S. Uddin: Thermosensitive polymer (N-isopropylacrylamide) coated nanomagnetic particles: Preparation and characterization, Colloids Surf. B **55**, 51–58 (2007) doi:10.1016/j.colsurfb.2006.11.007

11.154 D. Maharaj, B. Bhushan: Friction, wear and mechanical behavior of nano-objects on the nanoscale, Mater. Sci. Eng. R. **95**, 1–43 (2015) doi:10.1016/j.mser.2015.07.001

11.155 D. Maharaj, B. Bhushan: Scale effects of nanomechanical properties and deformation behavior of Au nanoparticle and thin film using depth sensing nanoindentation, Beilstein J. Nanotechnol. **5**, 822–836 (2014) doi:10.3762/bjnano.5.94

11.156 D. Mordehai, S.W. Lee, B. Backes, D.J. Srolovitz, W.D. Nix, E. Rabkin: Size effect in compression of single-crystal gold microparticles, Acta Mater. **59**, 5202–5215 (2011) doi:10.1016/j.actamat.2011.04.057

11.157 M. Ramos, L. Ortiz-Jordan, A. Hurtado-Macias, S. Flores, J.T. Elizalde-Galindo, C. Rocha, B. Torres, M. Zarei-Chaleshtori, R.R. Chianelli: Hardness and elastic modulus on six-fold symmetry gold nanoparticles, Materials **6**, 198–205 (2013) doi:10.3390/ma6010198

11.158 D.R. Saha, A. Mandal, S. Mitra, M.R. Mada, P. Boughton, S. Bandyopadhyay, D. Chakravorty: Nanoindentation studies on silver nanoparticles, Proc. Int. Conf. Recent Trends in Appl. Phys. Mater. Sci. **1536**, 257–258 (2013) doi:10.1063/1.4810198

11.159 H. Conrad, K. Jung: Effect of grain size from millimeters to nanometers on the flow stress and deformation kinetics of Ag, Mater. Sci. Eng. A **391**, 272–284 (2005) doi:10.1016/j.msea.2004.08.073

11.160 B. Chen, H. Zhang, K.A. Dunphy-Guzman, D. Spagnoli, M.B. Kruger, D.V.S. Muthu, M. Kunz, S. Fakra, J.Z. Hu, Q.Z. Guo, J.F. Banfield: Size-dependent elasticity of nanocrystalline titania, Phys. Rev. B **79**, 125406 (2009) doi:10.1103/PhysRevB.79.125406

11.161 D. Guo, G.X. Xie, J.B. Luo: Mechanical properties of nanoparticles: Basics and applications, J. Phys. D-Appl. Phys. **47**(1), 3001 (2014) doi:10.1088/0022-3727/47/1/013001

11.162 P. Paik, K.K. Kar, D. Deva, A. Sharma: Measurement of mechanical properties of polymer nanospheres by atomic force microscopy: Effects of particle size, Micro Nano Lett. **2**, 72–77 (2007) doi:10.1049/mnl:20070030

11.163 S.S. Tan, R.L. Sherman, W.T. Ford: Nanoscale compression of polymer microspheres by atomic force microscopy, Langmuir **20**, 7015–7020 (2004) doi:10.1021/la049597c

11.164 D. Maharaj, B. Bhushan: Effect of spherical Au nanoparticles on nanofriction and wear reduction in dry and liquid environments, Beilstein J. Nanotechnol. **3**, 759–772 (2012) doi:10.3762/bjnano.3.85

11.165 D. Guo, J.N. Li, L. Chang, J.B. Luo: Measurement of the friction between single polystyrene nanospheres and silicon surface using atomic force microscopy, Langmuir **29**, 6920–6925 (2013) doi:10.1021/la400984d

11.166 E. Gnecco, R. Bennewitz, T. Gyalog, C. Loppacher, M. Bammerlin, E. Meyer, H.J. Guntherodt: Velocity dependence of atomic friction, Phys. Rev. Lett. **84**, 1172–1175 (2000) doi:10.1103/PhysRevLett.84.1172

11.167 U. Simon, G. Schon, G. Schmid: The application of Au-55 clusters as quantum dots, Angewandte Chemie **32**, 250–254 (1993) doi:10.1002/anie.199302501

11.168 D.L. Klein, P.L. McEuen, J.E.B. Katari, R. Roth, A.P. Alivisatos: An approach to electrical studies of single nanocrystals, Appl. Phys. Lett. **68**, 2574–2576 (1996) doi:10.1063/1.116188

11.169 M. De, P.S. Ghosh, V.M. Rotello: Applications of nanoparticles in biology, Adv. Mater. **20**, 4225–4241 (2008) doi:10.1002/adma.200703183

11.170 T.A.P. Rocha-Santos: Sensors and biosensors based on magnetic nanoparticles, Trac-Trends Anal. Chem. **62**, 28–36 (2014) doi:10.1016/j.trac.2014.06.016

11.171 Y.P. Li, B. Srinivasan, Y. Jing, X.F. Yao, M.A. Hugger, J.P. Wang, C.G. Xing: Nanomagnetic competition assay for low-abundance protein biomarker quantification in unprocessed human sera, J. Am. Chem. Soc. **132**, 4388–4392 (2010) doi:10.1021/ja910406a

11.172 J. Panyam, V. Labhasetwar: Biodegradable nanoparticles for drug and gene delivery to cells and tissue, Adv. Drug Delivery Rev. **64**, 61–71 (2012) doi:10.1016/j.addr.2012.09.023

11.173 M.P. Desai, V. Labhasetwar, G.L. Amidon, R.J. Levy: Gastrointestinal uptake of biodegradable microparticles: Effect of particle size, Pharm. Res. **13**, 1838–1845 (1996) doi:10.1023/A:1016085108889

11.174 D. Peer, J.M. Karp, S. Hong, O.C. Faro Kzad, R. Margalit, R. Langer: Nanocarriers as an emerging platform for cancer therapy, Nat. Nanotechnol. **2**, 751–760 (2007) doi:10.1038/nnano.2007.387

11.175 X.Z. He, J.Y. Ma, A.E. Mercado, W.J. Xu, E. Jabbari: Cytotoxicity of paclitaxel in biodegradable self-assembled core-shell poly(lactide-co-glycolide ethylene oxide fumarate) nanoparticles, Pharm. Res. **25**, 1552–1562 (2008) doi:10.1007/s11095-007-9513-z

11.176 O.S. Wolfbeis: An overview of nanoparticles commonly used in fluorescent bioimaging, Chem. Soc. Rev. **44**, 4743–4768 (2015) doi:10.1039/c4cs00392f

11.177 M.K. So, C.J. Xu, A.M. Loening, S.S. Gambhir, J.H. Rao: Self-illuminating quantum dot conjugates for in vivo imaging, Nat. Biotechnol. **24**, 339–343 (2006) doi:10.1038/nbt1188

11.178 J. Estelrich, M.J. Sanchez-Martin, M.A. Busquets: Nanoparticles in magnetic resonance imaging: from simple to dual contrast agents, Int. J. Nanomed. **10**, 1727–1741 (2015) doi:10.2147/IJN.S76501

11.179 H.B. Na, I.C. Song, T. Hyeon: Inorganic nanoparticles for MRI contrast agents, Adv. Mater. **21**, 2133–2148 (2009) doi:10.1002/adma.200802366

11.180 C.J. Jia, F. Schuth: Colloidal metal nanoparticles as a component of designed catalyst, Phys. Chem. Chem. Phys. **13**, 2457–2487 (2011) doi:10.1039/c0cp02680h

11.181 M. Adlim, M.A. Bakar, K.Y. Liew, J. Ismail: Synthesis of chitosan-stabilized platinum and palladium nanoparticles and their hydrogenation activity, J. Mol. Catalysis A **212**, 141–149 (2004) doi:10.1016/j.molcata.2003.08.012

11.182 M. Ruta, N. Semagina, L. Kiwi-Minsker: Monodispersed Pd nanoparticles for acetylene selective hydrogenation: Particle size and support effects, J. Phys. Chem. C **112**, 13635–13641 (2008) doi:10.1021/jp803800w

11.183 K.M. Bratlie, H. Lee, K. Komvopoulos, P.D. Yang, G.A. Somorjai: Platinum nanoparticle shape effects on benzene hydrogenation selectivity, Nano Lett. **7**, 3097–3101 (2007) doi:10.1021/nl0716000

11.184 N. Dimitratos, J.A. Lopez-Sanchez, J.M. Anthonykutty, G. Brett, A.F. Carley, R.C. Tiruvalam, A.A. Herzing, C.J. Kiely, D.W. Knight, G.J. Hutchings: Oxidation of glycerol using gold-palladium alloy-supported nanocrystals, Phys. Chem. Chem. Phys. **11**, 4952–4961 (2009) doi:10.1039/b904317a

11.185 A.H. Battez, R. Gonzalez, J.L. Viesca, J.E. Fernandez, J.M.D. Fernandez, A. Machado, R. Chou, J. Riba: CuO, ZrO_2 and ZnO nanoparticles as antiwear additive in oil lubricants, Wear **265**, 422–428 (2008) doi:10.1016/j.wear.2007.11.013

11.186 X.B. Zhao, R.W. Long, Y. Chen, Z.G. Chen: Synthesis, characterization of Ce0(2)@Si0(2) nanoparticles and their oxide CMP behavior, Microelectron. Eng. **87**, 1716–1720 (2010) doi:10.1016/j.mee.2009.09.012

11.187 Y.C. Kang, S.L.I. Chan: Tensile properties of nanometric Al203 particulate-reinforced aluminum matrix composites, Mater. Chem. Phys. **85**, 438–443 (2004) doi:10.1016/j.matchemphys.2004.02.002

11.188 J. Jiao, X. Sun, T.J. Pinnavaia: Mesostructured silica for the reinforcement and toughening of rubbery and glassy epoxy polymers, Polymer **50**, 983–989 (2009) doi:10.1016/j.polymer.2008.12.042

11.189 J.E. Millstone, D.F.J. Kavulak, C.H. Woo, T.W. Holcombe, E.J. Westling, A.L. Briseno, M.F. Toney, J.M.J. Frechet: Synthesis, properties, and electronic applications of size-controlled poly(3-hexylthiophene) nanoparticles, Langmuir **26**, 13056–13061 (2010) doi:10.1021/la1022938

11.190 Y.S. Ye, X.L. Xie, J. Rick, F.C. Chang, B.J. Hwang: Improved anode materials for lithium-ion batteries comprise non-covalently bonded graphene and silicon nanoparticles, J. Power Sources **247**, 991–998 (2014) doi:10.1016/j.jpowsour.2013.08.048

11.191 H.B. Gu, B. Jin, D.K. Jun, Z. Han: Improved electrochemical performance of LiCoP04 nanoparticles for lithium ion batteries, J. Nanosci. Nanotechnol. **7**, 4037–4040 (2007) doi:10.1166/jnn.2007.078

11.192 K.T. Lee, Y.S. Jung, S.M. Oh: Synthesis of tin-encapsulated spherical hollow carbon for anode material in lithium secondary batteries, J. Am. Chem. Soc. **125**, 5652–5653 (2003) doi:10.1021/ja0345524

11.193 A. Kumar, P.K. Vemula, P.M. Ajayan, G. John: Silver-nanoparticle-embedded antimicrobial paints based on vegetable oil, Nat. Mater. **7**, 236–241 (2008) doi:10.1038/nmat2099

11.194 J.S. Kim, E. Kuk, K.N. Yu, J.H. Kim, S.J. Park, H.J. Lee, S.H. Kim, Y.K. Park, Y.H. Park, C.Y. Hwang, Y.K. Kim, Y.S. Lee, D.H. Jeong, M.H. Cho: Antimicrobial effects of silver nanoparticles, Nanomed.-Nanotechnol. Biol. Med. **3**, 95–101 (2007) doi:10.1016/j.nano.2006.12.001

11.195 S. Baruah, M.N. Khan, J. Dutta: Perspectives and applications of nanotechnology in water treatment, Environ. Chem. Lett. **14**, 1–14 (2016) doi:10.1007/s10311-015-0542-2